Introduction to sparse-data X-ray tomography: Part B

Samuli Siltanen

Department of Mathematics and Statistics
University of Helsinki, Finland
samuli.siltanen@helsinki.fi
www.siltanen-research.net

IMPA, Rio de Janeiro, Brazil
Symposium on Inverse Problems in Science and Engineering
October 24–27, 2017

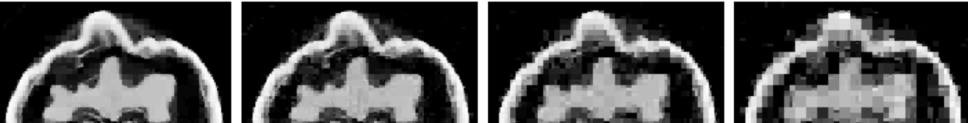

Finnish Centre of Excellence in Inverse Modelling and Imaging

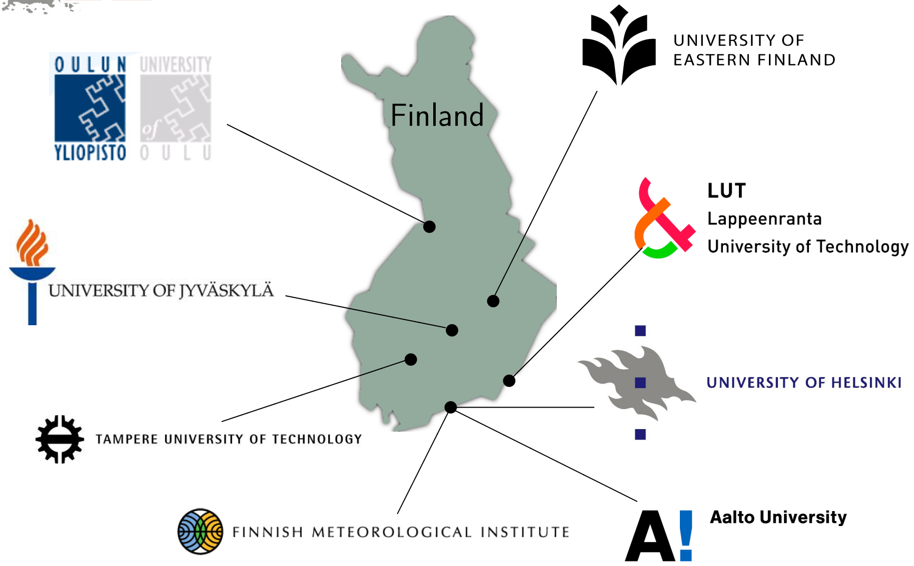

Course team

Markus Juvonen

Alexander Meaney

Matlab instruction: please ask Alexander or Markus!
The session is after Friday's lecture.

Links to open computational resources

Open CT datasets:

- Finnish Inverse Problems Society (FIPS) dataset page

Matrix-based parallel-beam reconstruction algorithms:
FIPS Computational Blog

- Truncated SVD
- Total Variation regularization

Matrix-free large-scale reconstruction algorithms:

- Matlab page of Mueller-S 2012 book
- ASTRA toolbox
- TVReg: Software for 3D Total Variation Regularization

Outline

Hospital case study: diagnosing osteoarthritis

Controlled wavelet-domain sparsity (CWDS)

From wavelet bases to shearlet frames

Remark on back-projection, or the transpose matrix A^T

Limited angle tomography

Industrial case study: low-dose 3D dental X-ray imaging

This is a joint work with

Tatiana Bubba, University of Helsinki, Finland

Sakari Karhula, Oulu University Hospital, Finland

Juuso Ketola, Oulu University Hospital, Finland

Maximilian März, TU Berlin

Miika T. Nieminen, University of Oulu, Finland

Zenith Purisha, University of Helsinki, Finland

Juho Rimpeläinen, University of Helsinki, Finland

Simo Saarakkala, Oulu University Hospital, Finland

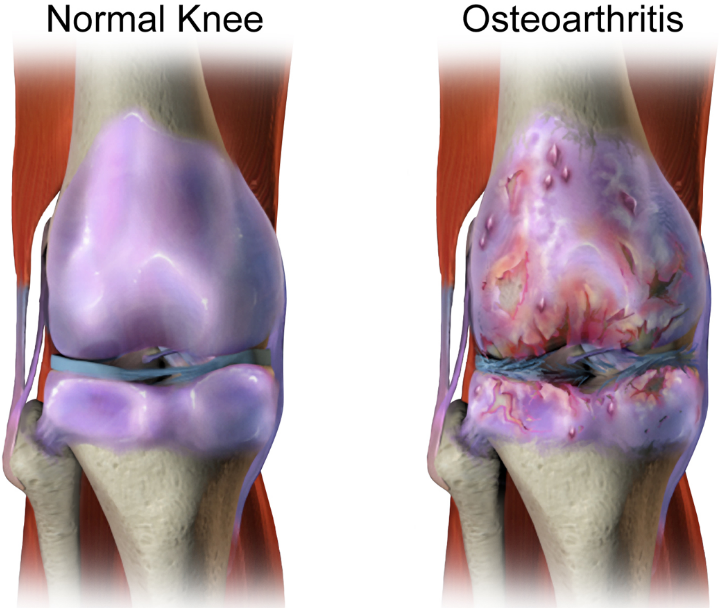
Normal Knee
Osteoarthritis

We consider small specimens of human bone imaged using microtomography

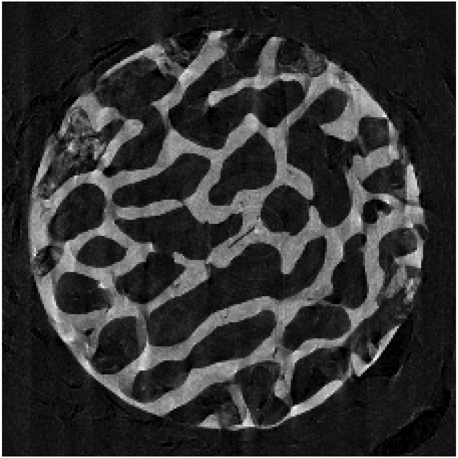

Slice of 3D reconstruction by FDK based on **596 angles**

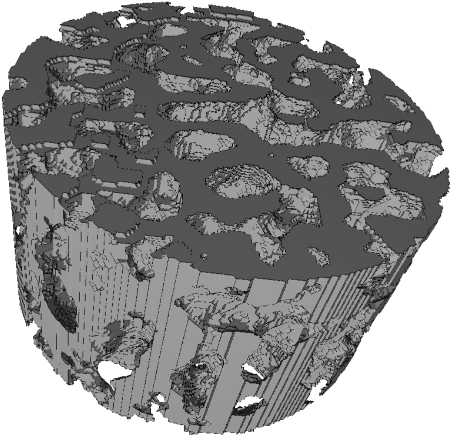

Three-dimensional structure

We pick out a smaller region of interest for osteoarthritis analysis

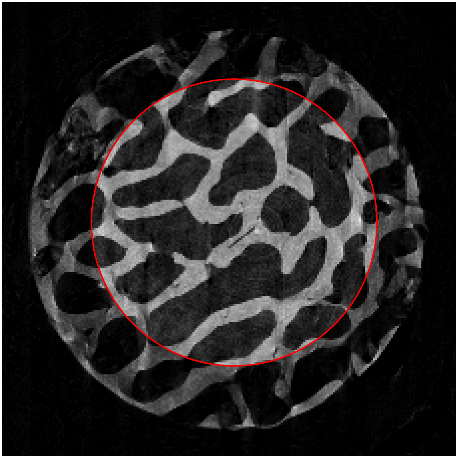

Slice of 3D reconstruction by FDK based on **596 angles**

Slice of 3D region of interest after binary thresholding

We use two numerical quality measures applied to segmented three-dimensional bone structure

Trabecular thickness

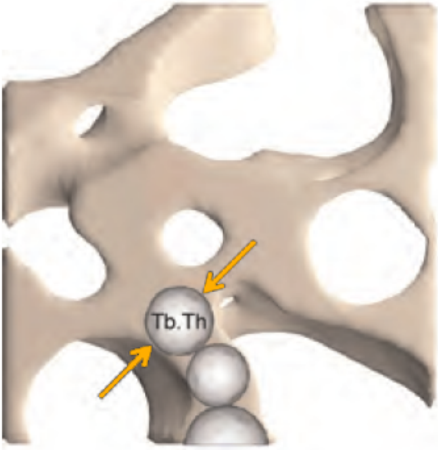

Trabecular separation

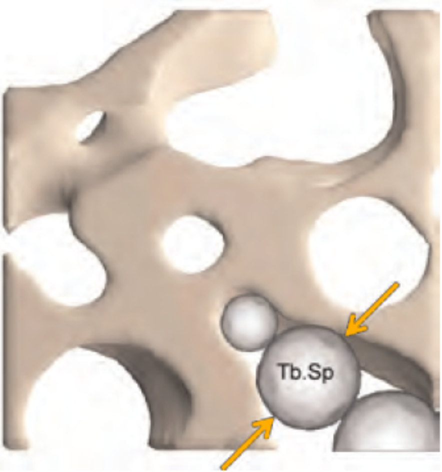

[Bouxsein, Boyd, Christiansen, Guldberg, Jepsen, & Müller 2010]

The goal is to reduce measurement time by recording fewer radiographs

3D FDK reconstruction
based on **40 angles**

3D shearlet-sparsity reconstruction
based on **40 angles**

Bone quality parameters from ground truth

Healthy bone

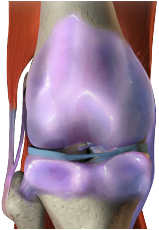

Osteoarthritic bone

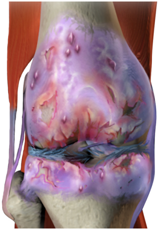

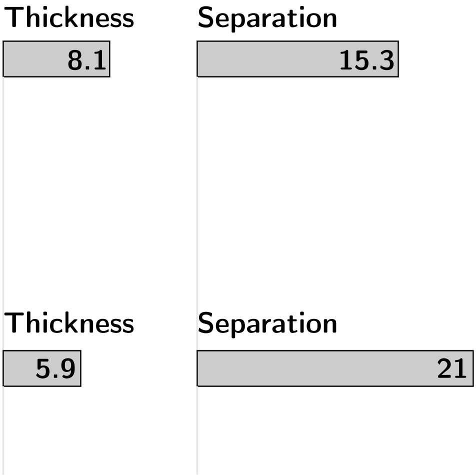

[Purisha, Karhula, Rimpeläinen, Nieminen, Saarakkala & S, submitted]

Results from FDK reconstructions

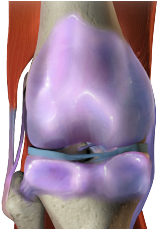

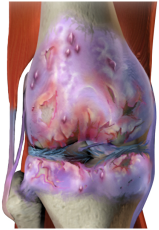

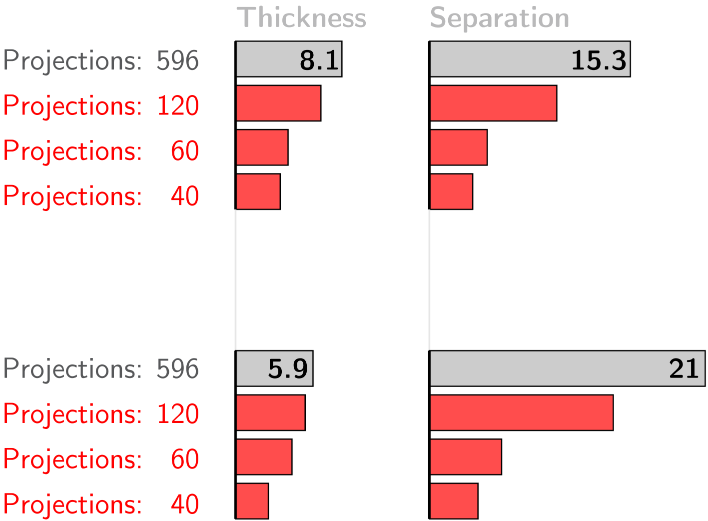

[Purisha, Karhula, Rimpeläinen, Nieminen, Saarakkala & S, submitted]

Results from 3D shearlet-sparsity reconstructions

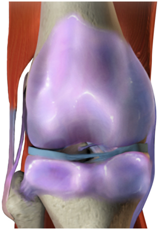

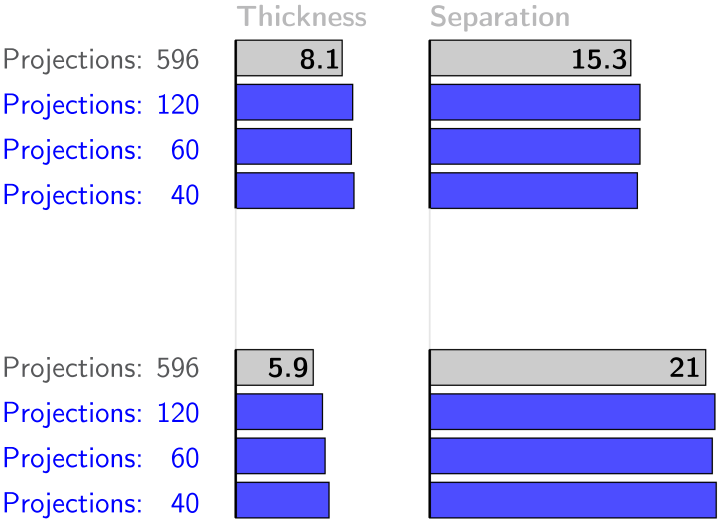

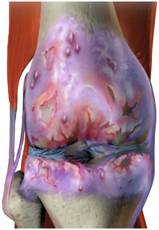

[Purisha, Karhula, Rimpeläinen, Nieminen, Saarakkala & S, submitted]

Outline

Hospital case study: diagnosing osteoarthritis

Controlled wavelet-domain sparsity (CWDS)

From wavelet bases to shearlet frames

Remark on back-projection, or the transpose matrix A^T

Limited angle tomography

Industrial case study: low-dose 3D dental X-ray imaging

Daubechies, Defrise and de Mol introduced a revolutionary inversion method in 2004

Consider the sparsity-promoting variational regularization

$$\underset{f\in\mathbb{R}^n}{\arg\min}\left\{\|Af-m\|_2^2+\mu\|Wf\|_1\right\},$$

where W is an orthonormal wavelet transform. The minimizer can be computed using the iteration

$$f_{j+1}=W^{-1}S_\mu W\left(f_j+A^T(m-Af_j)\right),$$

where the soft-thresholding operation

$$S_\mu(x)=\begin{cases}x+\frac{\mu}{2} & \text{if } x\leq-\frac{\mu}{2},\\ 0 & \text{if } |x|<\frac{\mu}{2},\\ x-\frac{\mu}{2} & \text{if } x\geq\frac{\mu}{2},\end{cases}$$

is applied to each wavelet coefficient separately.

We modify the method so that non-negativity constraint has rigorous mathematical foundation

The minimizer

$$\operatorname*{argmin}_{f\in\mathbb{R}^n_+}\left\{\frac{1}{2}\|Af-m\|_2^2+\mu\,\|Wf\|_1\right\}$$

can be computed using this iteration:

$$\begin{aligned}
y^{(i+1)} &= \mathbb{P}_C\Big(f^{(i)}-\tau\nabla g(f^{(i)})-\lambda W^T v^{(i)}\Big)\\
v^{(i+1)} &= \Big(I-S_\mu\Big)\Big(Wy^{(i+1)}+v^{(i)}\Big)\\
f^{(i+1)} &= \mathbb{P}_C\Big(f^{(i)}-\tau\nabla g(f^{(i)})-\lambda W^T v^{(i+1)}\Big)
\end{aligned}$$

where $\tau>0$, $\lambda>0$ and $g(f)=\frac{1}{2}\|Af-m\|_2^2$. Here $\mathbb{P}_C$ denotes projection to the non-negative "quadrant."

[Loris & Verhoeven 2011], [Chen, Huang & Zhang 2016]

Illustration of the Haar wavelet transform

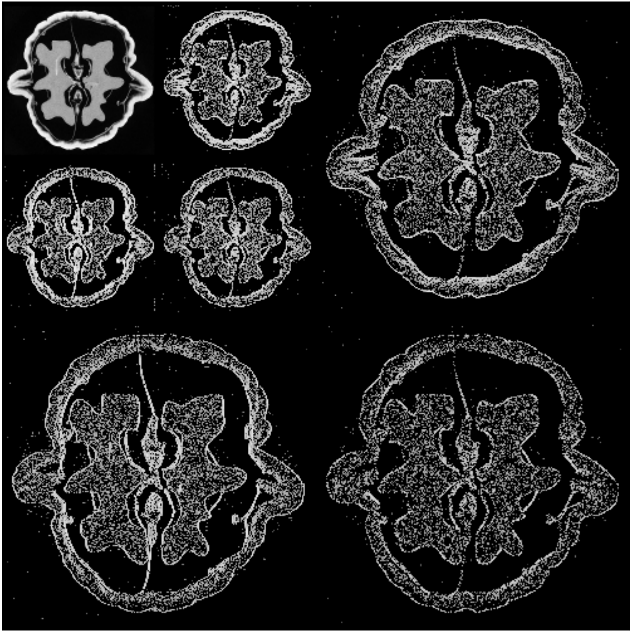

Sparse-data reconstruction of the walnut using Haar wavelet sparsity

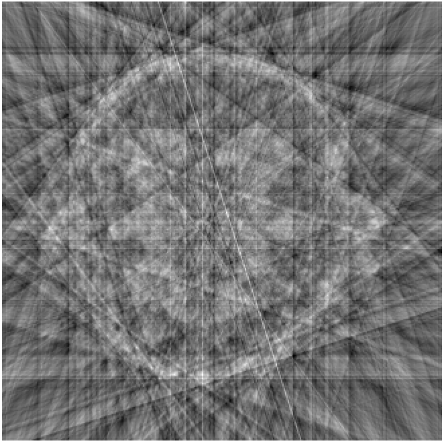

Filtered back-projection

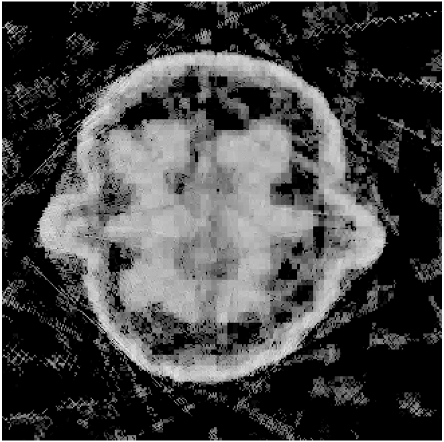

Constrained Besov regularization

$$\arg\min_{f\in\mathbb{R}^n_+}\left\{\|Af-m\|_2^2+\alpha\|f\|_{B^1_{11}}\right\}$$

How to choose the thresholding parameter μ? Here it is too small.

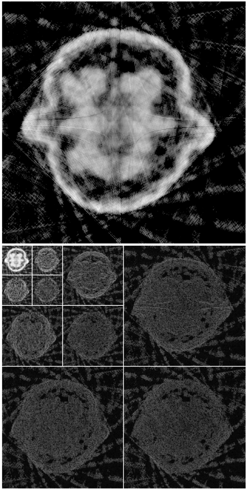

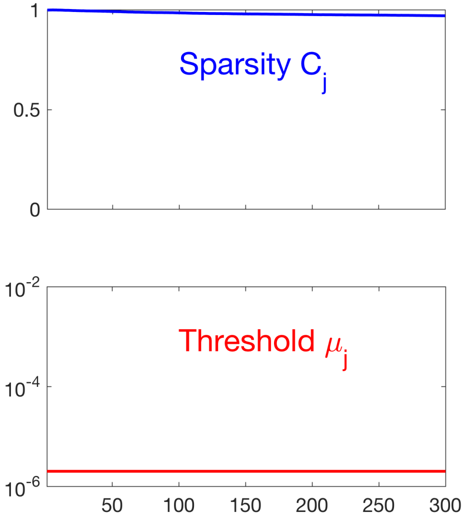

How to choose the thresholding parameter μ? Here it is too large.

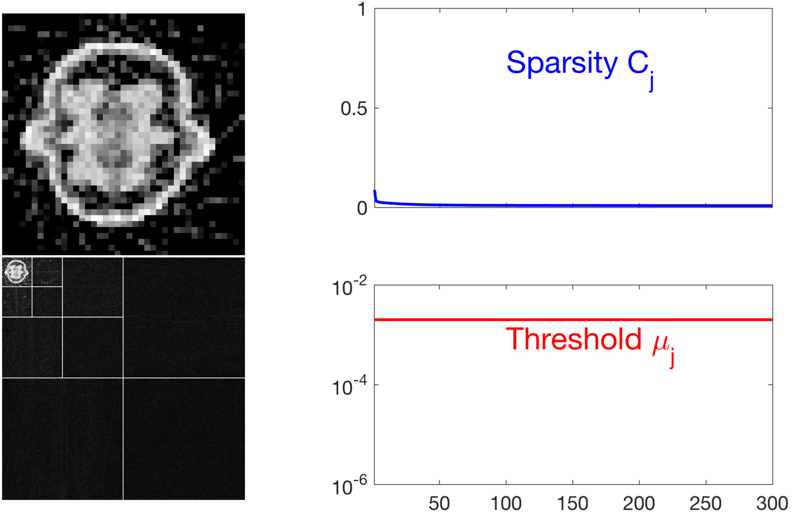

Automatic parameter choice using controlled wavelet-domain sparsity (CWDS)

Assume given the *a priori* sparsity level $0 \leq \mathcal{C}_{\text{pr}} \leq 1$.
Denote by $\mathcal{C}_j$ the sparsity of the jth iterate $f_j \in \mathbb{R}^n$:

$$\mathcal{C}_j = (\text{number of nonzero elements in } Wf_j \in \mathbb{R}^n)/n.$$

The CWDS iteration is based on proportional-integral-derivative (PID) controllers:

$$\mu^{(i+1)} = \mu^{(i)} + \beta(\mathcal{C}^{(i)} - \mathcal{C}_{\text{pr}}).$$

[Purisha, Rimpeläinen, Bubba & S, arXiv:1703.09798, to appear in *Measurement Science and Technology.*]

CWDS choice of the thresholding parameter μ

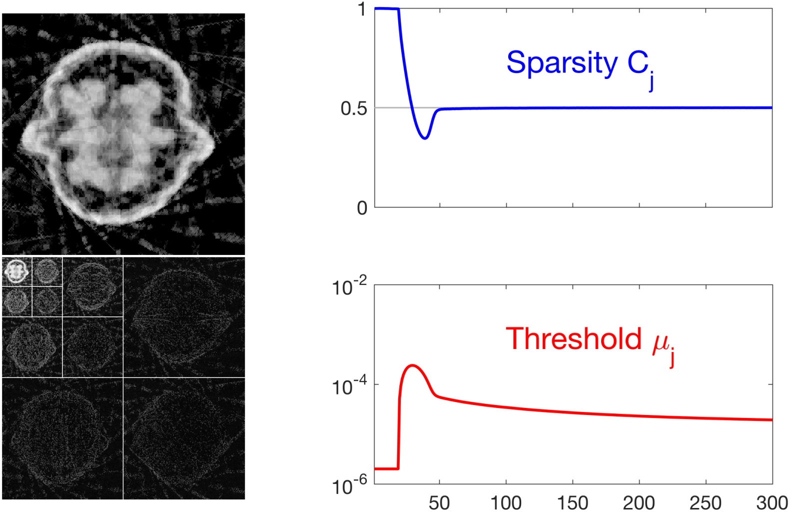

CWDS choice of the thresholding parameter μ

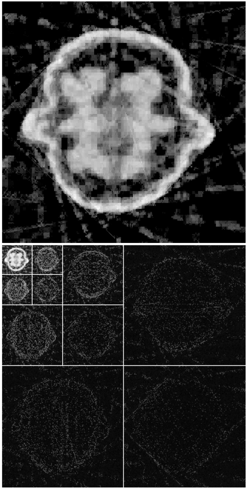

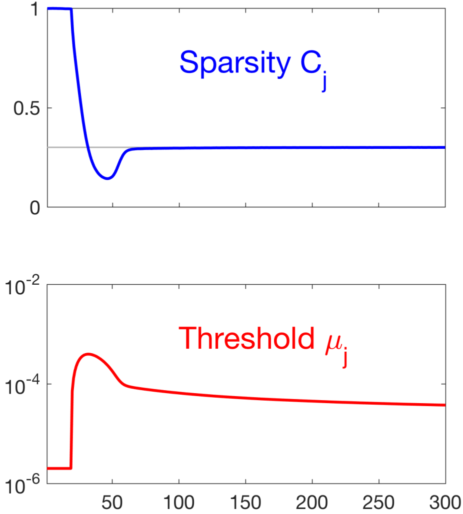

CWDS choice of the thresholding parameter μ

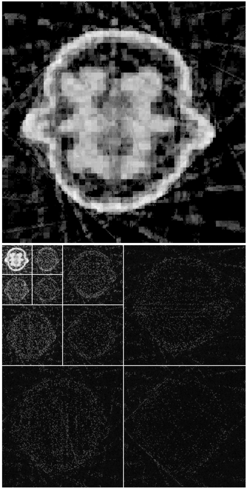

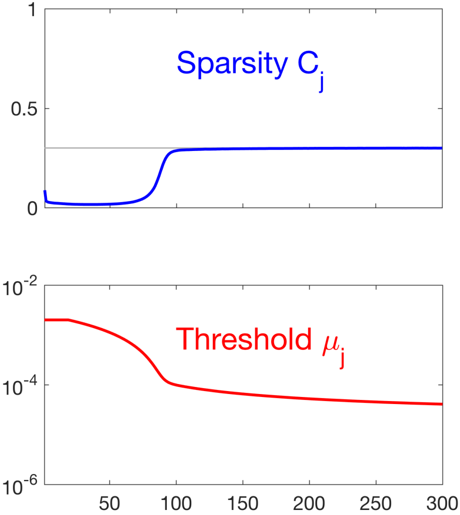

Outline

Hospital case study: diagnosing osteoarthritis

Controlled wavelet-domain sparsity (CWDS)

From wavelet bases to shearlet frames

Remark on back-projection, or the transpose matrix A^T

Limited angle tomography

Industrial case study: low-dose 3D dental X-ray imaging

Shearlet coefficients at coarse scale 1/8

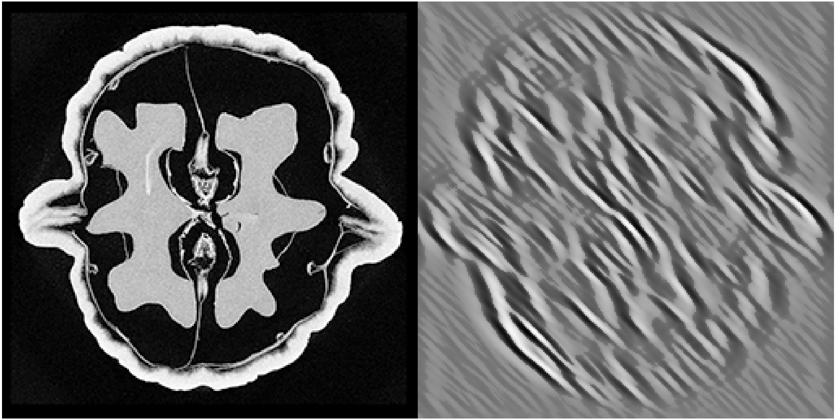

We use Shearlab [Kutyniok, Shahram & Zhuang 2012].

Shearlet coefficients at coarse scale 2/8

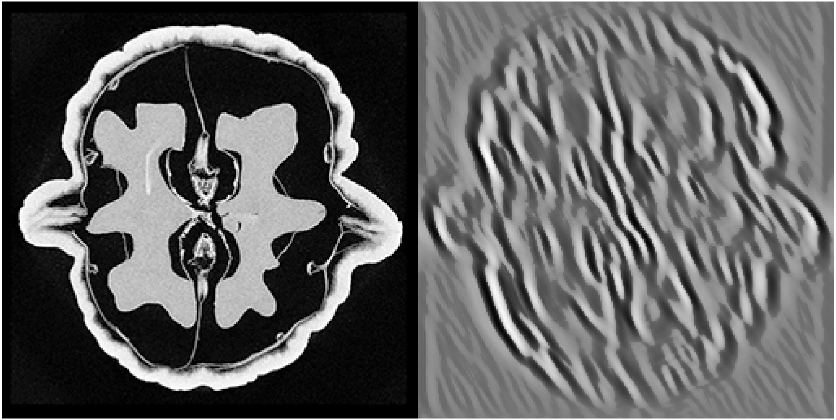

We use Shearlab [Kutyniok, Shahram & Zhuang 2012].

Shearlet coefficients at coarse scale 3/8

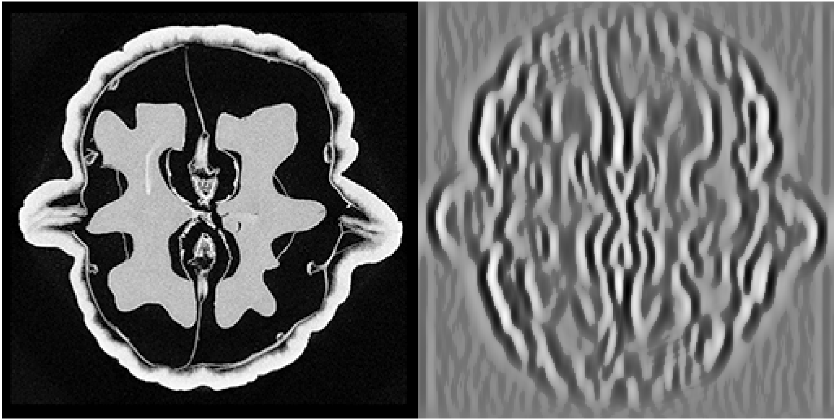

We use Shearlab [Kutyniok, Shahram & Zhuang 2012].

Shearlet coefficients at coarse scale 4/8

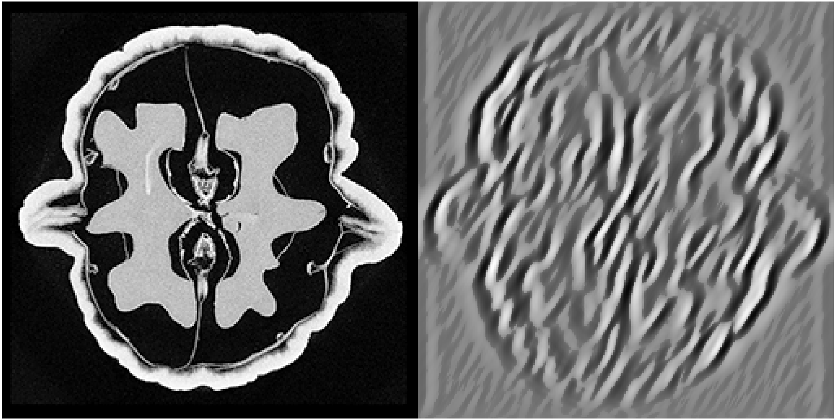

We use Shearlab [Kutyniok, Shahram & Zhuang 2012].

Shearlet coefficients at coarse scale 5/8

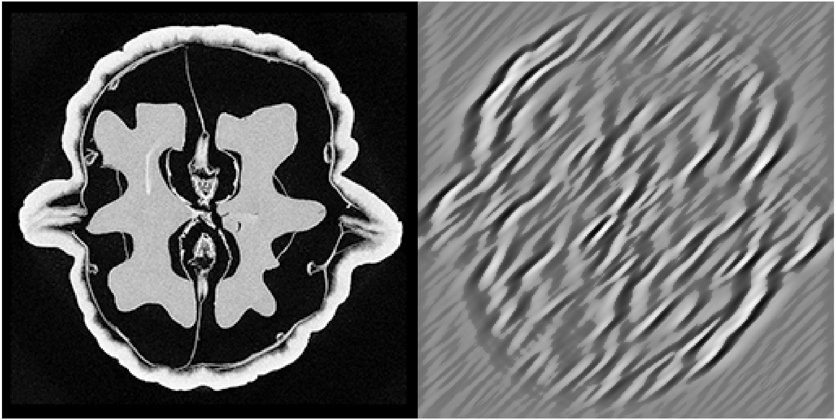

We use Shearlab [Kutyniok, Shahram & Zhuang 2012].

Shearlet coefficients at coarse scale 6/8

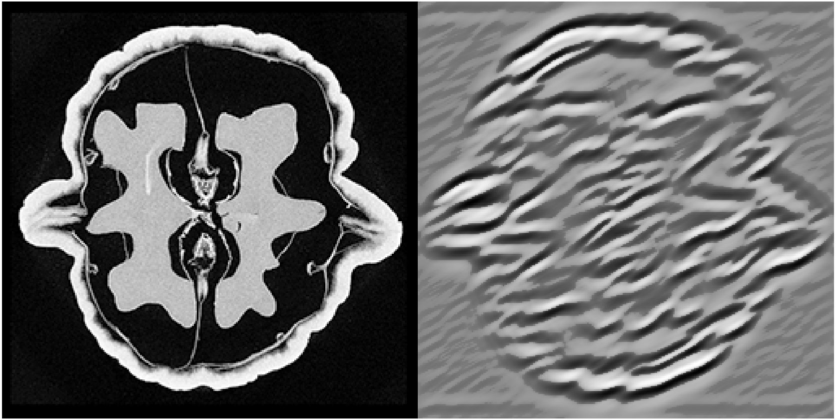

We use Shearlab [Kutyniok, Shahram & Zhuang 2012].

Shearlet coefficients at coarse scale 7/8

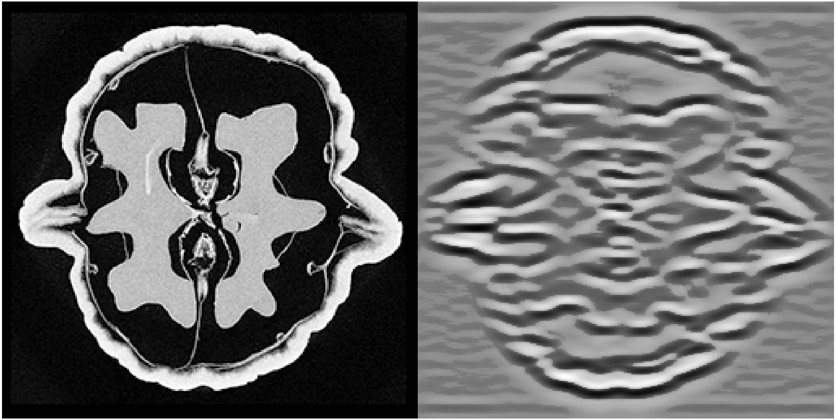

We use Shearlab [Kutyniok, Shahram & Zhuang 2012].

Shearlet coefficients at coarse scale 8/8

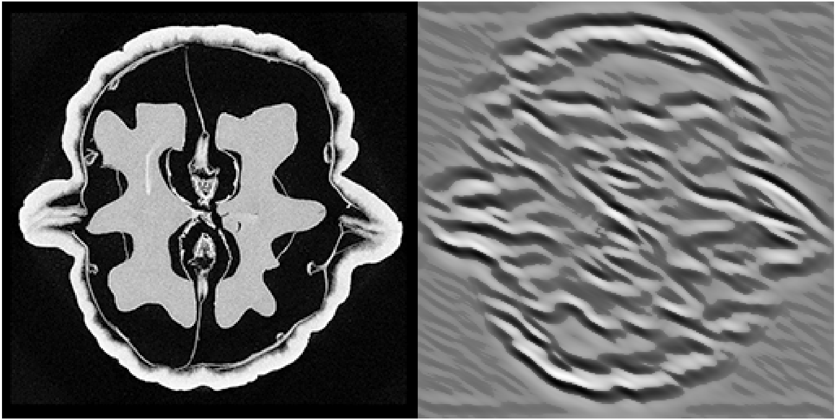

We use Shearlab [Kutyniok, Shahram & Zhuang 2012].

Shearlet coefficients at medium scale 1/8

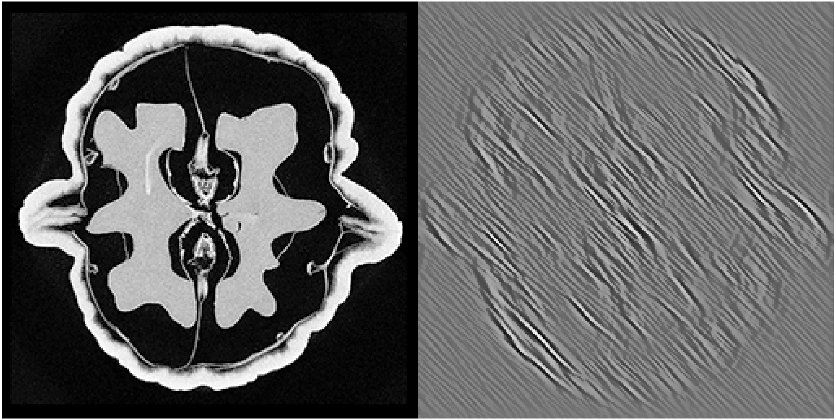

We use Shearlab [Kutyniok, Shahram & Zhuang 2012].

Shearlet coefficients at medium scale 2/8

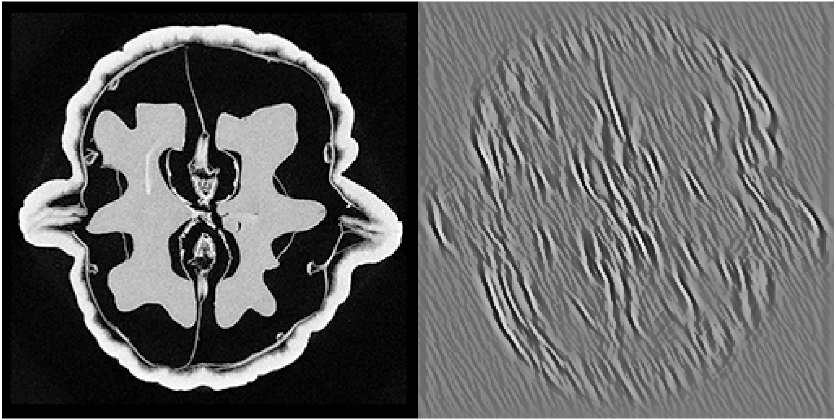

We use Shearlab [Kutyniok, Shahram & Zhuang 2012].

Shearlet coefficients at medium scale 3/8

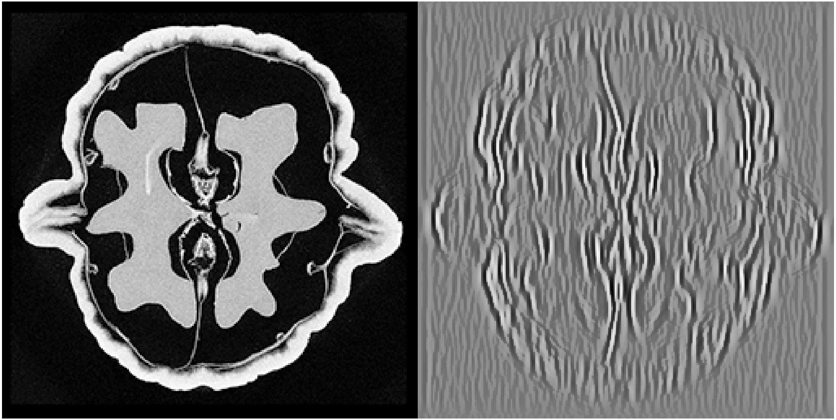

We use Shearlab [Kutyniok, Shahram & Zhuang 2012].

Shearlet coefficients at medium scale 4/8

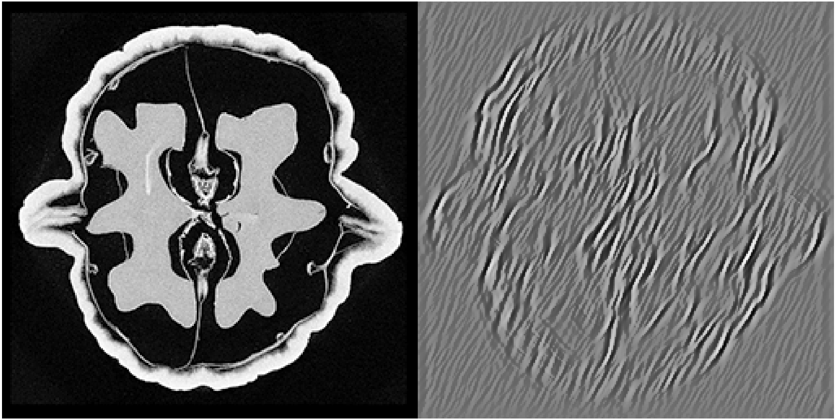

We use Shearlab [Kutyniok, Shahram & Zhuang 2012].

Shearlet coefficients at medium scale 5/8

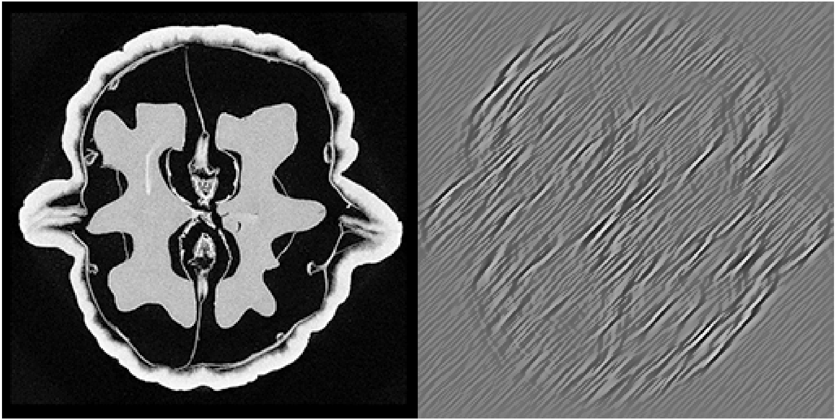

We use Shearlab [Kutyniok, Shahram & Zhuang 2012].

Shearlet coefficients at medium scale 6/8

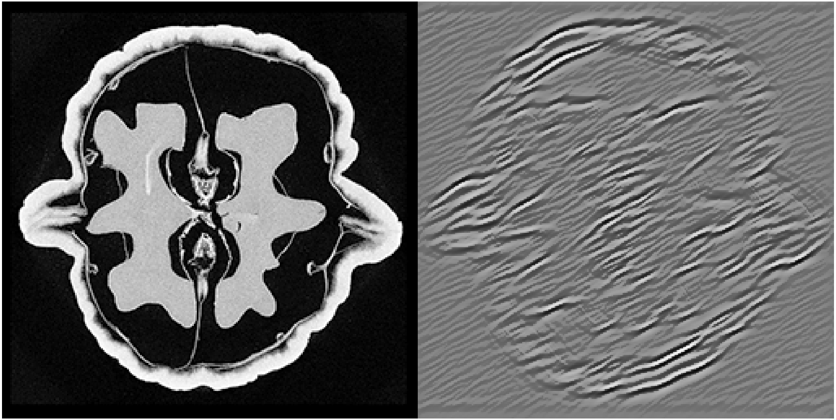

We use Shearlab [Kutyniok, Shahram & Zhuang 2012].

Shearlet coefficients at medium scale 7/8

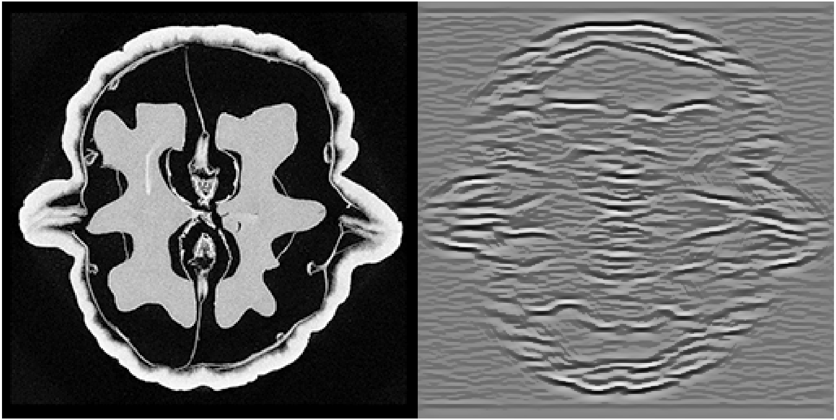

We use Shearlab [Kutyniok, Shahram & Zhuang 2012].

Shearlet coefficients at medium scale 8/8

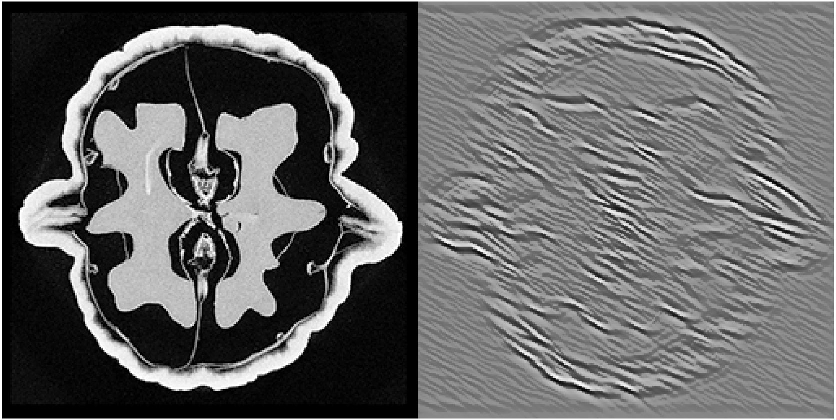

We use Shearlab [Kutyniok, Shahram & Zhuang 2012].

Shearlet coefficients at fine scale 1/16

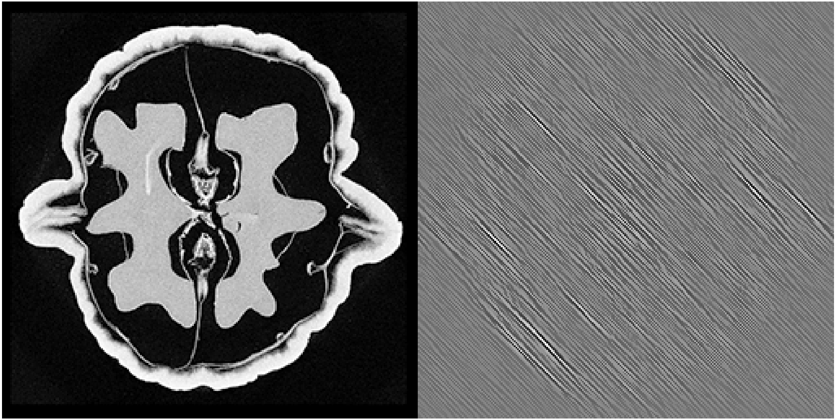

We use Shearlab [Kutyniok, Shahram & Zhuang 2012].

Shearlet coefficients at fine scale 2/16

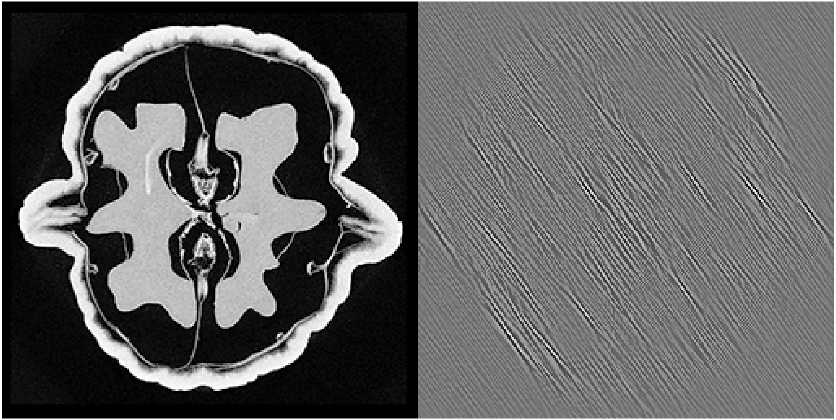

We use Shearlab [Kutyniok, Shahram & Zhuang 2012].

Shearlet coefficients at fine scale 3/16

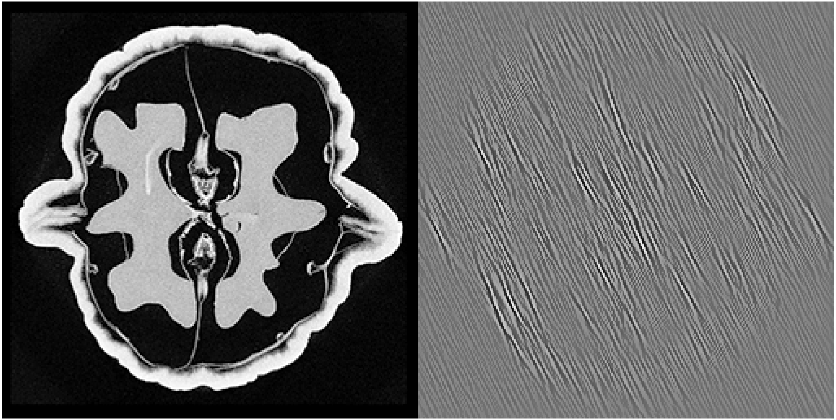

We use Shearlab [Kutyniok, Shahram & Zhuang 2012].

Shearlet coefficients at fine scale 4/16

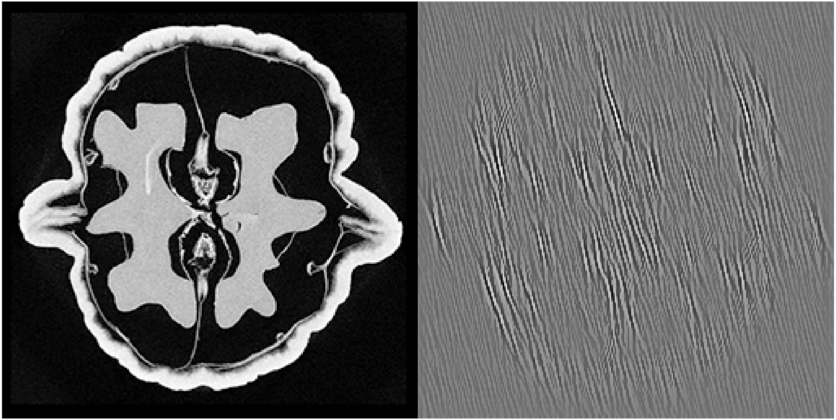

We use Shearlab [Kutyniok, Shahram & Zhuang 2012].

Shearlet coefficients at fine scale 5/16

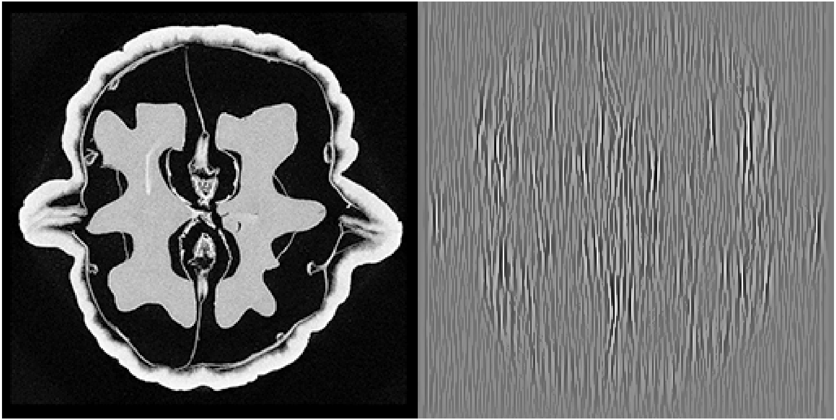

We use Shearlab [Kutyniok, Shahram & Zhuang 2012].

Shearlet coefficients at fine scale 6/16

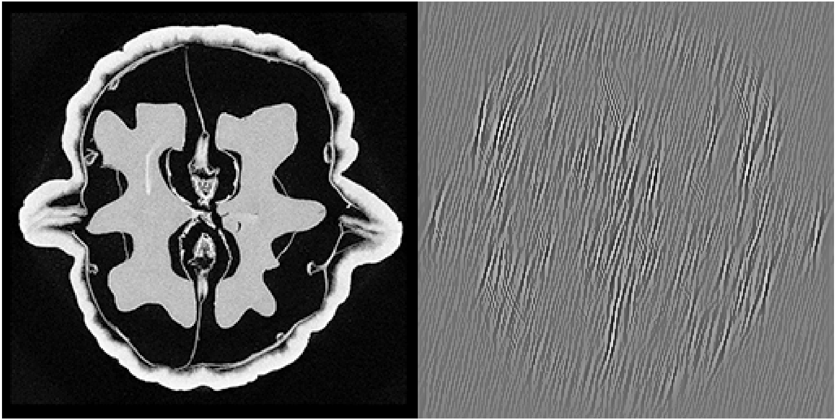

We use Shearlab [Kutyniok, Shahram & Zhuang 2012].

Shearlet coefficients at fine scale 7/16

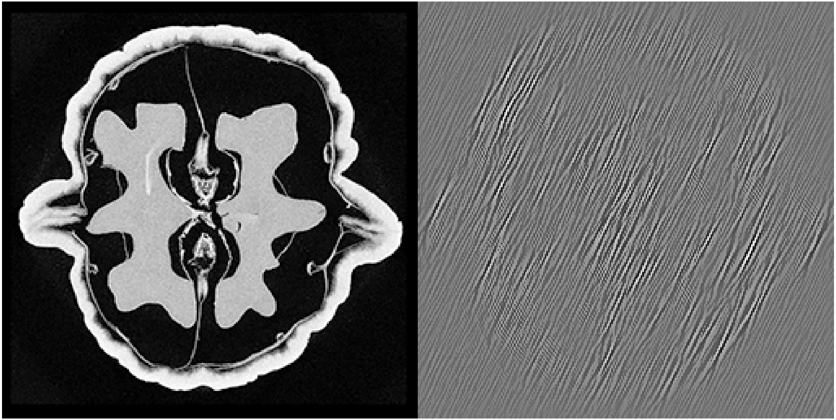

We use Shearlab [Kutyniok, Shahram & Zhuang 2012].

Shearlet coefficients at fine scale 8/16

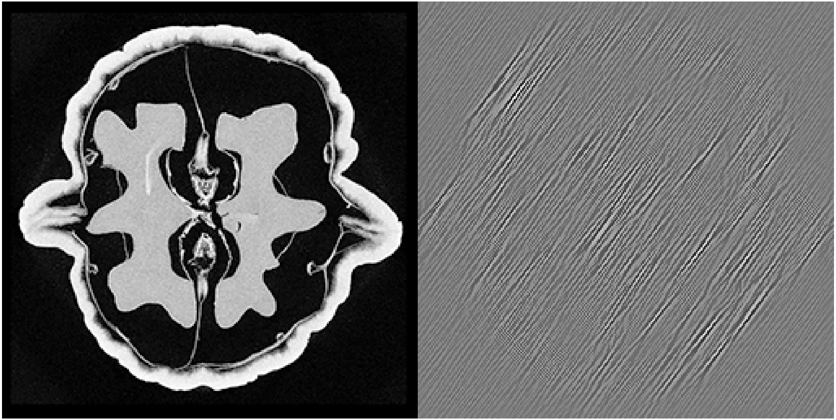

We use Shearlab [Kutyniok, Shahram & Zhuang 2012].

Shearlet coefficients at fine scale 9/16

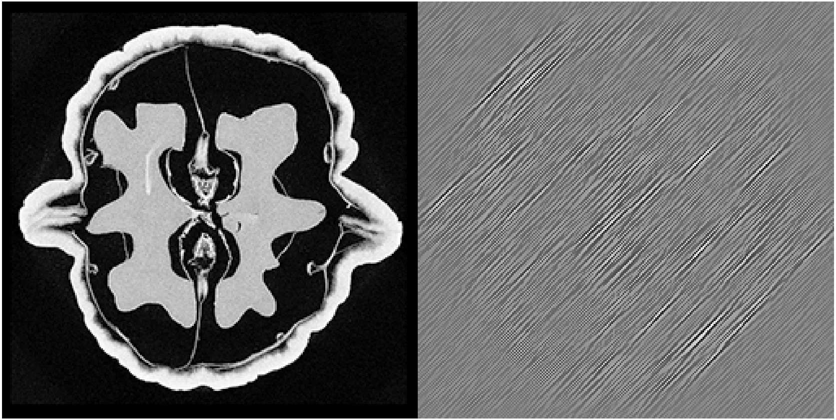

We use Shearlab [Kutyniok, Shahram & Zhuang 2012].

Shearlet coefficients at fine scale 10/16

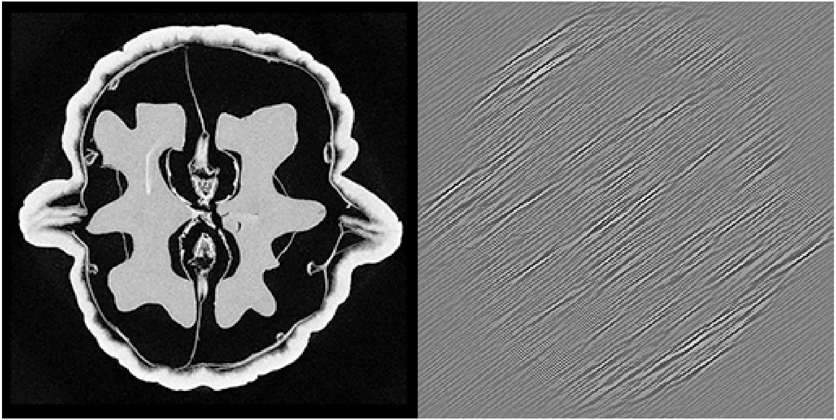

We use Shearlab [Kutyniok, Shahram & Zhuang 2012].

Shearlet coefficients at fine scale 11/16

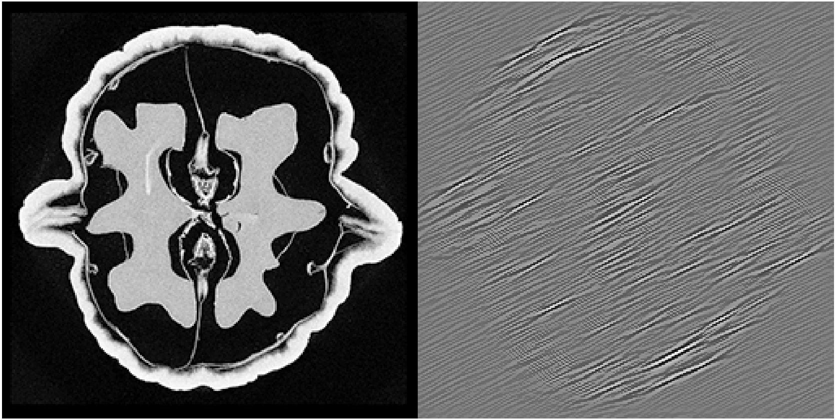

We use Shearlab [Kutyniok, Shahram & Zhuang 2012].

Shearlet coefficients at fine scale 12/16

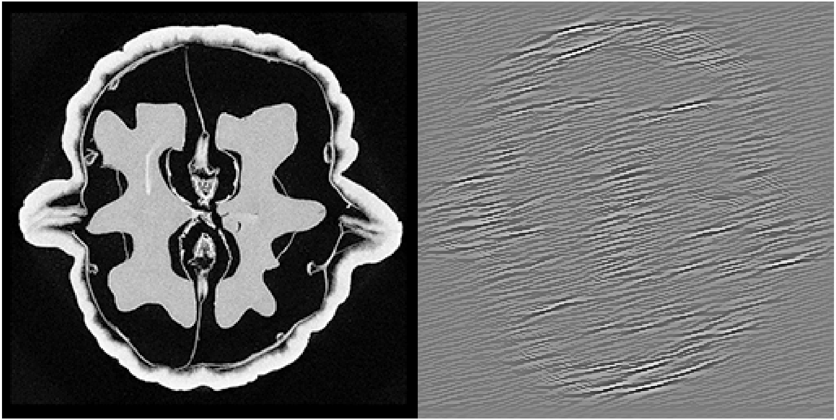

We use Shearlab [Kutyniok, Shahram & Zhuang 2012].

Shearlet coefficients at fine scale 13/16

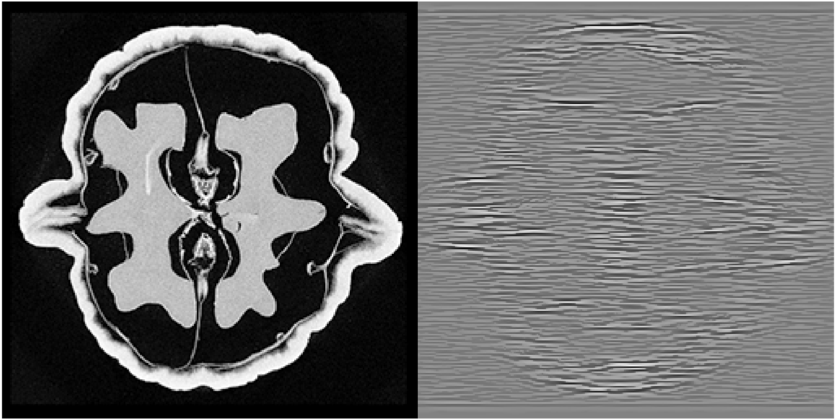

We use Shearlab [Kutyniok, Shahram & Zhuang 2012].

Shearlet coefficients at fine scale 14/16

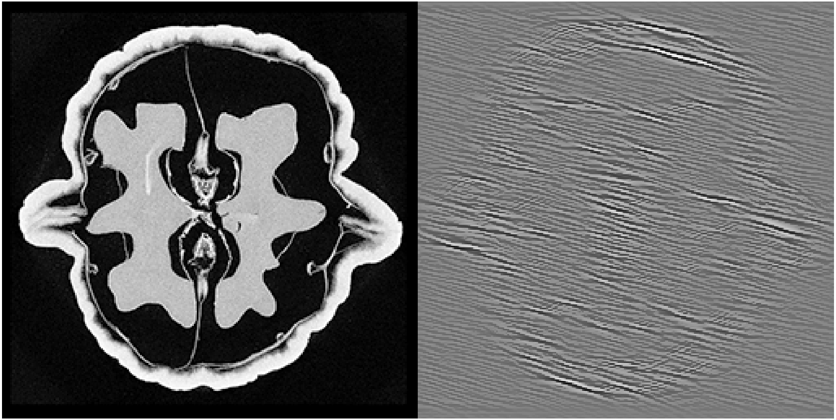

We use Shearlab [Kutyniok, Shahram & Zhuang 2012].

Shearlet coefficients at fine scale 15/16

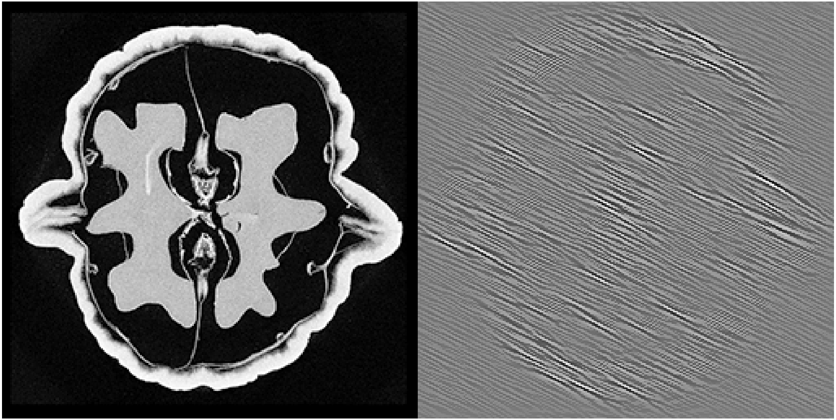

We use Shearlab [Kutyniok, Shahram & Zhuang 2012].

Shearlet coefficients at fine scale 16/16

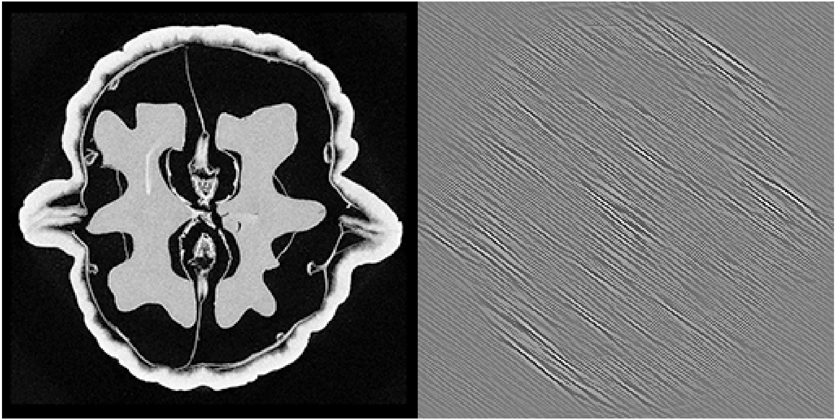

We use Shearlab [Kutyniok, Shahram & Zhuang 2012].

The shearlet transform gives multi-resolution and orientation-aware building blocks for image data

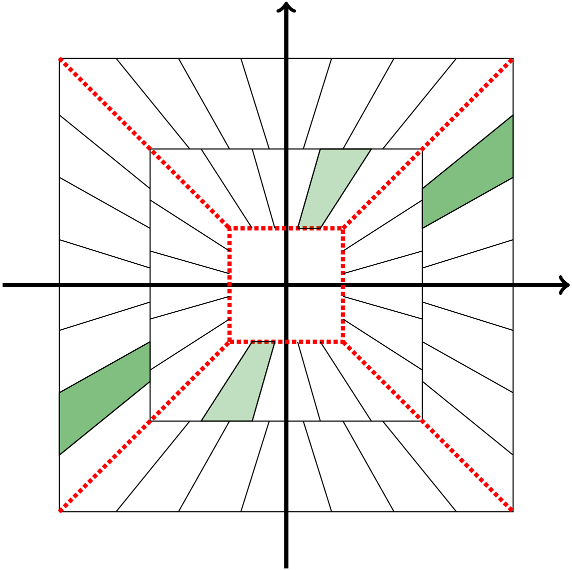

Schematic diagram of the frequency plane tiling of several elements of a 2D shearlet system, for different values of dilation and shearing parameters.

Sparse-data reconstruction of the walnut using shearlet sparsity

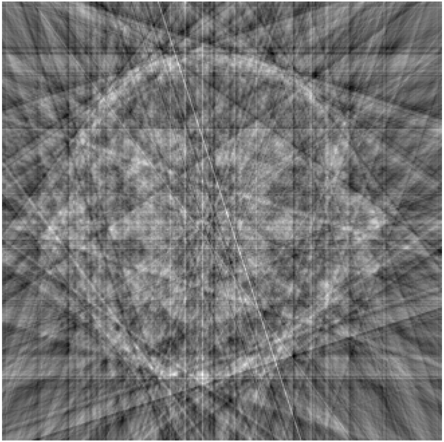

Filtered back-projection

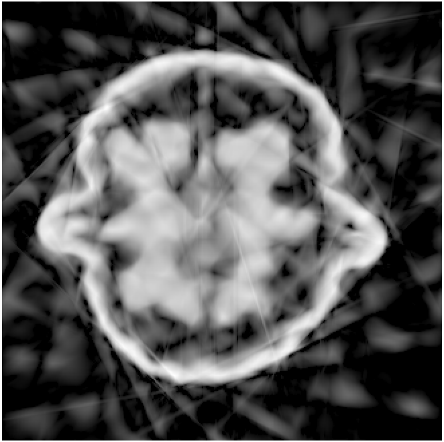

Shearlet-sparse reconstruction, with transform code from `http://www.shearlab.org/`

Outline

Hospital case study: diagnosing osteoarthritis

Controlled wavelet-domain sparsity (CWDS)

From wavelet bases to shearlet frames

Remark on back-projection, or the transpose matrix A^T

Limited angle tomography

Industrial case study: low-dose 3D dental X-ray imaging

The transpose matrix A^T appears in many inversion methods, including Tikhonov regularization

Write a penalty functional

$$\Phi(f) = \|Af - m\|_2^2 + \alpha \|f\|_2^2,$$

where $0 < \alpha < \infty$ is a regularization parameter. Define $\Gamma_\alpha(m)$ by

$$\Phi(\Gamma_\alpha(m)) = \min_{f \in X} \{\Phi(f)\}.$$

We denote

$$\Gamma_\alpha(m) = \arg\min_{f \in X} \{\|Af - m\|_2^2 + \alpha \|f\|_2^2\}.$$

In large-scale computations it is better to use the formula

$$\Gamma_\alpha(m) = (A^T A + \alpha I)^{-1} A^T m.$$

Projected Barzilai-Borwein minimization

Denote $\|f\|_\beta := \sum_{i=1}^{n} \sqrt{(f_i)^2 + \beta}$ with $\beta > 0$. Minimize

$$G_\beta(f) := \frac{1}{2}\|Af - \widetilde{\mathbf{g}}\|_2^2 + \alpha\left(\|L_H f\|_\beta + \|L_V f\|_\beta\right),$$

with a non-negativity constraint:

$$f^{k+1} = P\left(f^k - \lambda_k \nabla G_\beta(f^k)\right), \quad k = 0, \ldots, k_{max} - 1.$$

The step size is

$$\lambda_k = \frac{(f^k - f^{k-1})^T (f^k - f^{k-1})}{(f^k - f^{k-1})^T (\nabla G_\beta(f^k) - \nabla G_\beta(f^{k-1}))}$$

and $P : \mathbb{R}^n \to \mathbb{R}^n$ is the projection

$$(P(f))_i = \begin{cases} f_i & \mathit{if}\, f_i \geq 0 \\ 0 & \mathit{if}\, f_i < 0 \end{cases}, \quad i = 1, \ldots, n.$$

Matlab code available at this page.

Loris and Verhoeven introduced an algorithm applicable to shearlet-sparsifying inversion

[Loris & Verhoeven 2011] The minimization of

$$\underset{f \in \mathbb{R}^n}{\arg\min} \left\{ \|Af - m\|_2^2 + \mu \|\mathcal{T} f\|_1 \right\}$$

can be computed using this iteration:

$$\begin{aligned} g_{j+1} &= f_j + A^T(m - Af_j), \\ w_{j+1} &= P_\mu \left(w_j + \mathcal{T}(g_{j+1} - \mathcal{T}^T w_j) \right), \\ f_{j+1} &= g_{j+1} - \mathcal{T}^T w_{j+1}, \end{aligned}$$

where $P_\mu(u) = u - \mathcal{S}_\mu$.

Let's take a closer look at the transpose A^T, also known as back-projection operator

Our tomographic matrix equation is $Af = m$, where

- $f \in \mathbb{R}^n$ is the target, and
- $m \in \mathbb{R}^k$ is the sinogram.

Target space

Sinogram space

$$\begin{tikzcd}
f \in \mathbb{R}^n \arrow[rr, "\text{projection } A"] & & \mathbb{R}^k \ni m \\
\mathbb{R}^n & & \mathbb{R}^k \arrow[ll, "\text{back-projection } A^T"']
\end{tikzcd}$$

Example of the action of A^T: point target

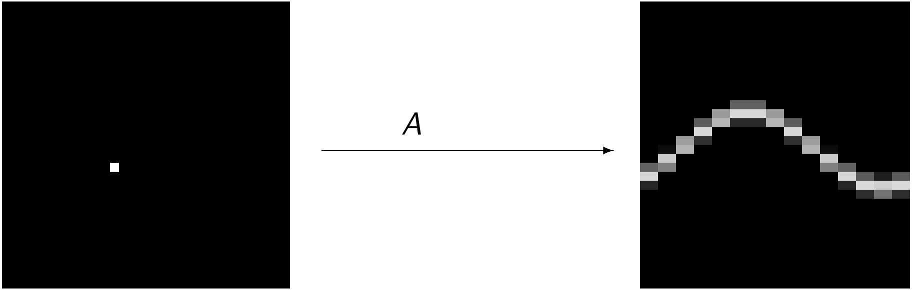

This is why A^T is called the back-projection

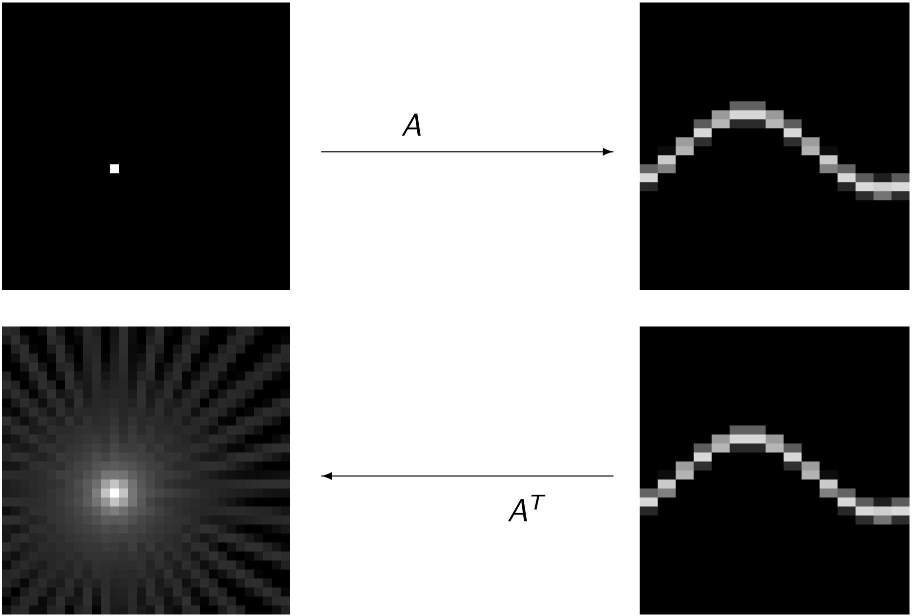

Example of the action of A^T: point sinogram

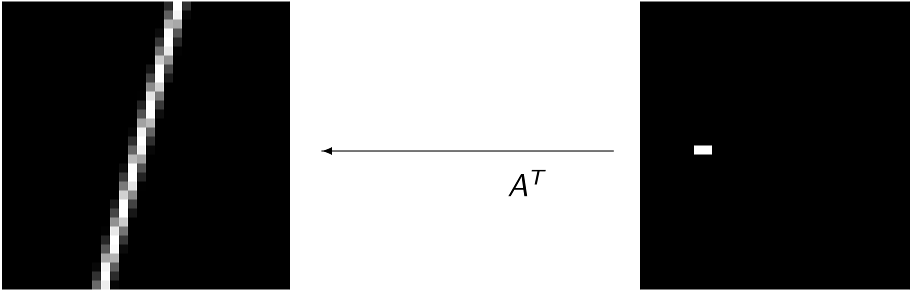

Here is another point sinogram

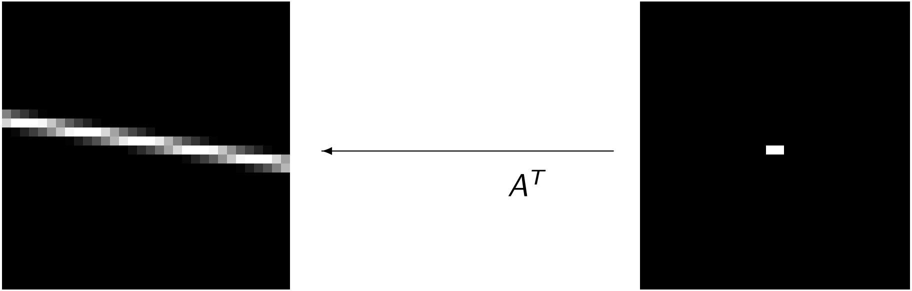

Rotating around the object allows us to form the so-called *sinogram*

https://www.youtube.com/watch?v=5Vyc1TzmNI8

Radon transform

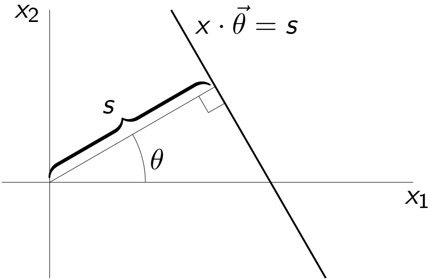

The most classical model for X-ray data is the *Radon transform*

$$Rf(\theta, s) = \int_{x \cdot \theta = s} f(x)dx = \int_{y \in \theta^\perp} f(s\theta + y)dy, \qquad \theta \in S^1, s \in \mathbb{R},$$

where S^1 is the unit circle, $\theta^\perp$ is the orthogonal complement of the unit vector θ, and $x \cdot \theta$ denotes vector inner product.

This is an illustration of the standard reconstruction by filtered back-projection

https://www.youtube.com/watch?v=ddZeLNh9aac

The back-projection operator

To reconstruct f at a point x, the most obvious data related to $f(x)$ are the integrals over lines passing through x. Let us sum them all together, call the result $Tf(x)$ and see what we get by introducing polar coordinates:

$$\begin{aligned} Tf(x) &= \int_0^{\pi} \int_{-\infty}^{\infty} f(x+t\theta)\,dt\,d\theta \\ &= \int_0^{2\pi} \int_0^{\infty} \frac{f(x+t\theta)}{t}\,t\,dt\,d\theta \\ &= \int_{\mathbb{R}^2} \frac{f(x+y)}{|y|}\,dy \\ &= \int_{\mathbb{R}^2} \frac{f(y)}{|x-y|}\,dy \\ &= \left(f(y) * \frac{1}{|y|}\right)(x), \end{aligned}$$

where $*$ stands for convolution.

Filtered back-projection

We want to find an inverse operator for T. Note that

$$\widehat{\frac{1}{|y|}}(\xi) = \frac{1}{|\xi|}.$$

Furthermore, define the Calderón operator Λ in all dimensions $\mathbb{R}^n$ by

$$\Lambda f(x) := \mathcal{F}^{-1}|\xi|\hat{f}(\xi) = \frac{1}{(2\pi)^n}\int_{\mathbb{R}^n} e^{ix\cdot\xi}|\xi|\hat{f}(\xi)d\xi, \qquad (1)$$

where $\mathcal{F}^{-1}$ is the inverse Fourier transform. Note that Λ can be thought of as a high-pass filter. Now we see that

$$\widehat{Tf}(\xi) = \frac{\hat{f}(\xi)}{|\xi|},$$

and therefore $f = \Lambda T f = \Lambda R^* R f$, where R^* is a dual operator of the Radon transform R. See Chapter II.2 of [Natterer 1986].

Outline

Hospital case study: diagnosing osteoarthritis

Controlled wavelet-domain sparsity (CWDS)

From wavelet bases to shearlet frames

Remark on back-projection, or the transpose matrix A^T

Limited angle tomography

Industrial case study: low-dose 3D dental X-ray imaging

Construction of limited-angle sinogram

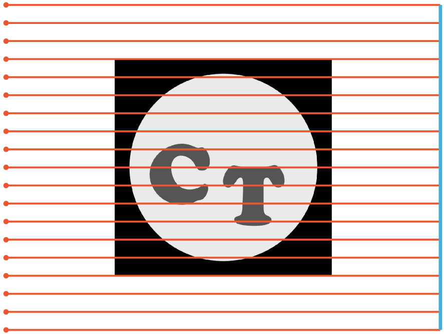

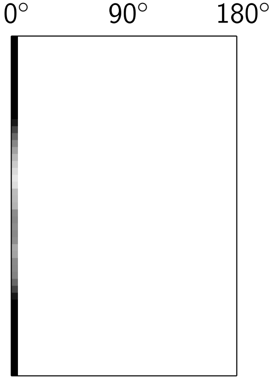

Construction of limited-angle sinogram

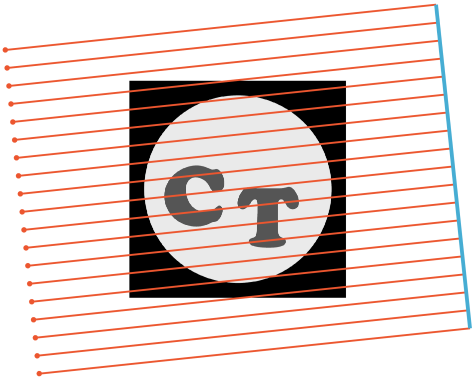

Construction of limited-angle sinogram

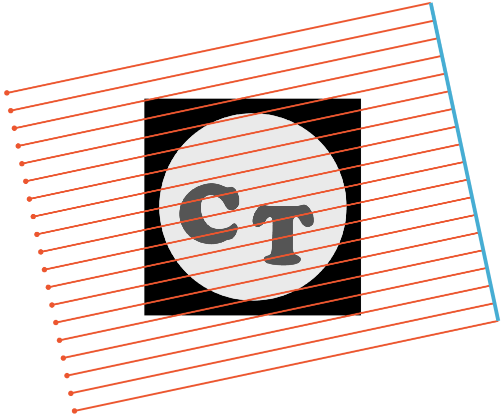

Construction of limited-angle sinogram

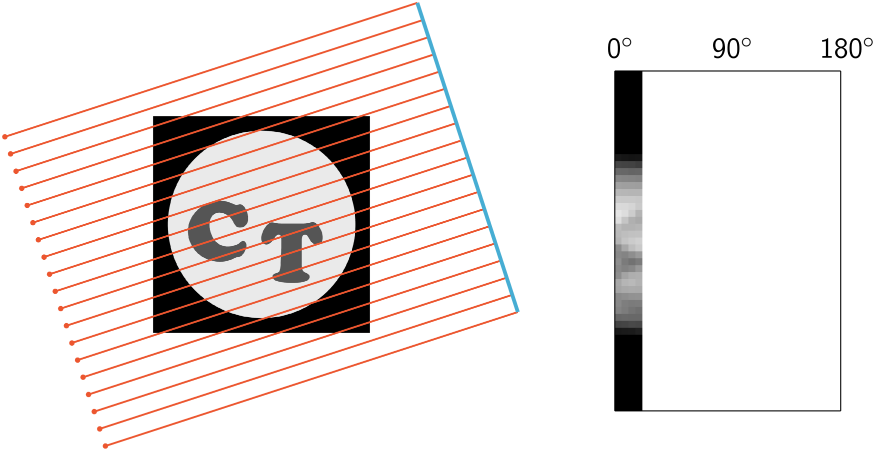

Construction of limited-angle sinogram

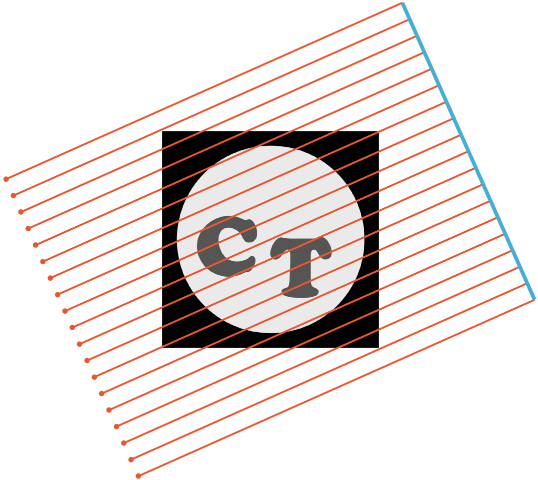

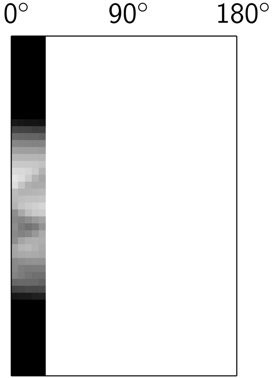

Construction of limited-angle sinogram

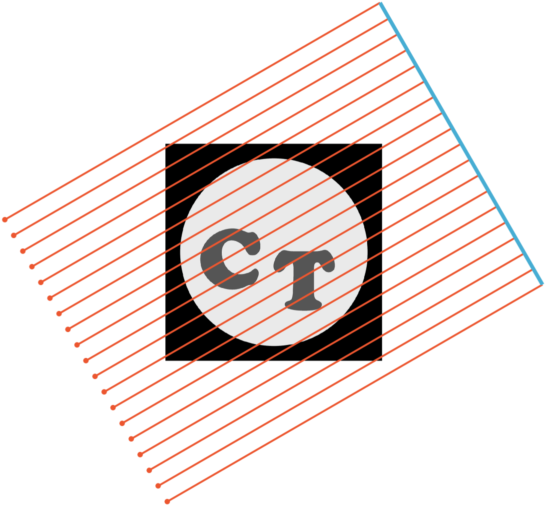

Construction of limited-angle sinogram

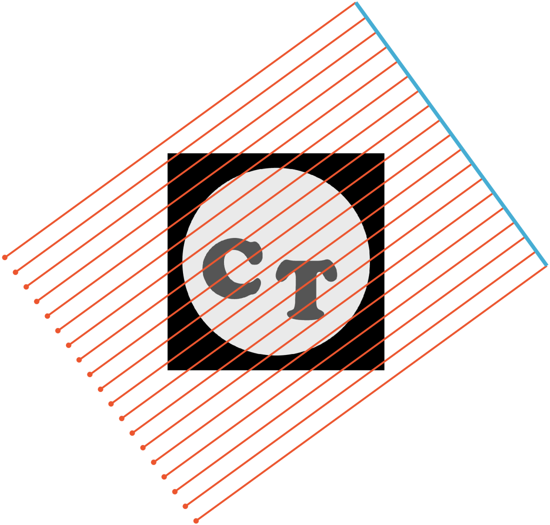

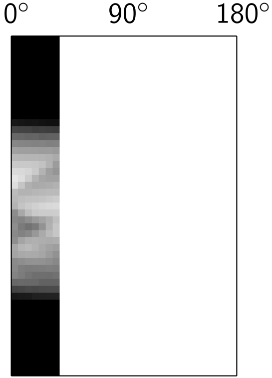

Construction of limited-angle sinogram

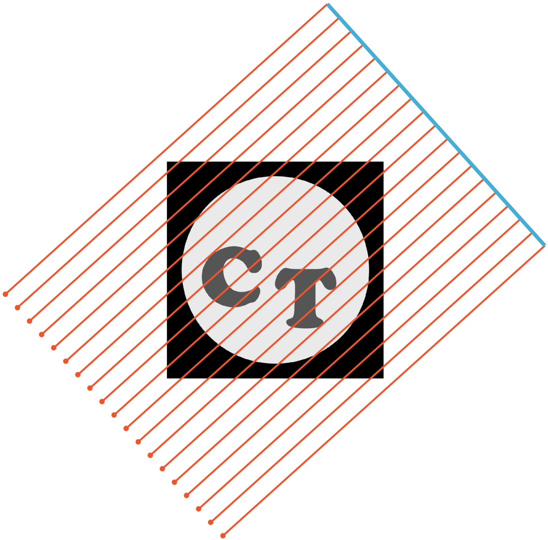

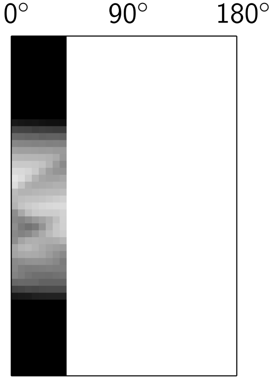

Construction of limited-angle sinogram

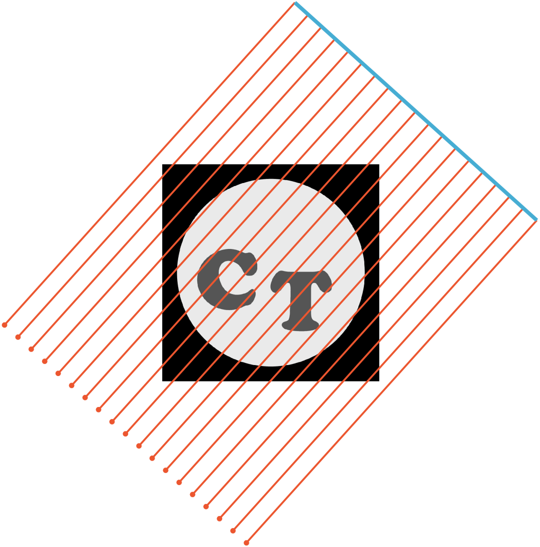

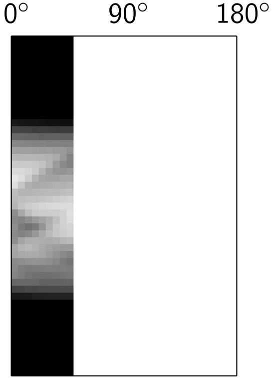

Construction of limited-angle sinogram

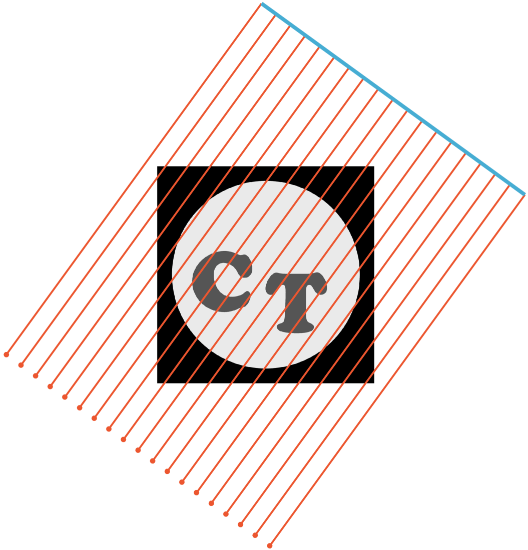

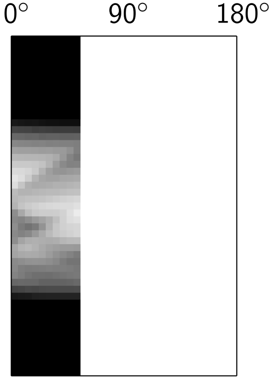

Construction of limited-angle sinogram

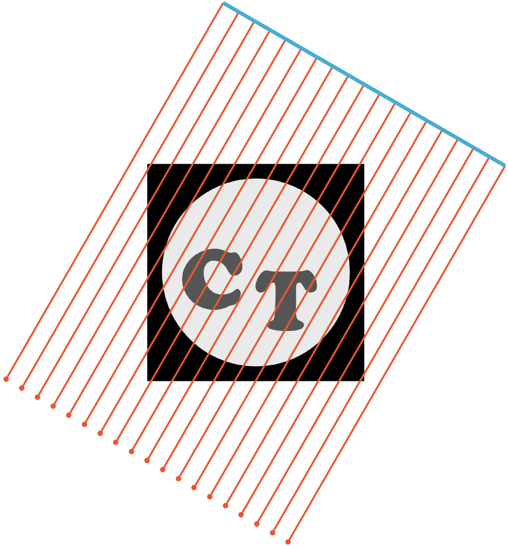

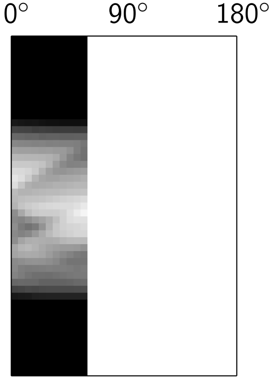

Construction of limited-angle sinogram

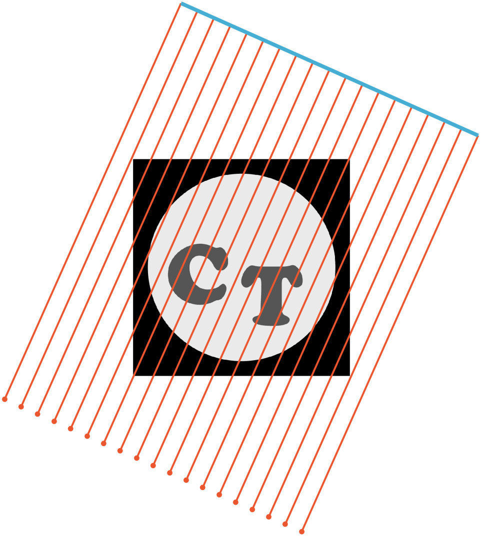

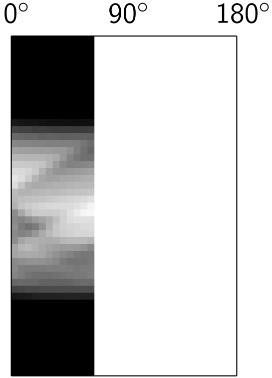

Construction of limited-angle sinogram

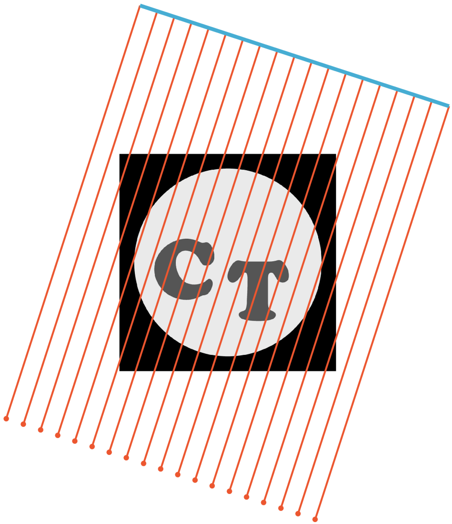

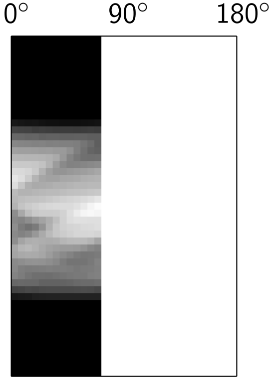

Construction of limited-angle sinogram

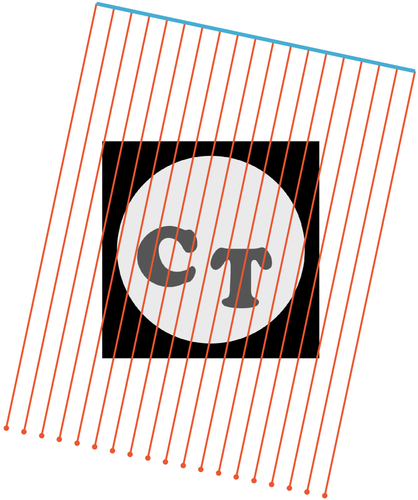

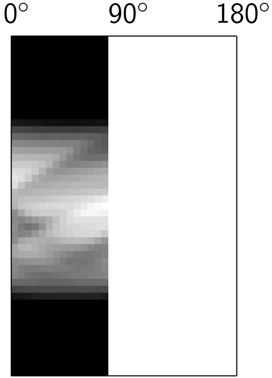

Construction of limited-angle sinogram

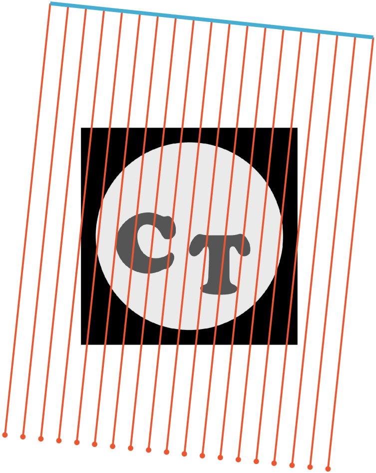

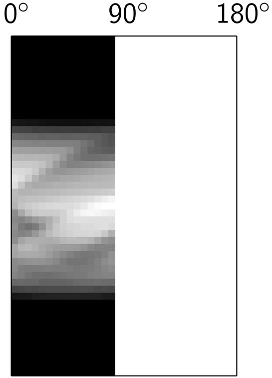

Singular value decomposition $A = U^T DV$

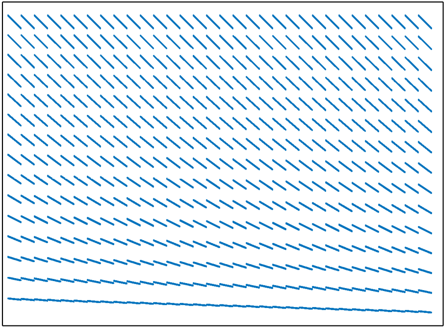

735×1024 system matrix A,
only nonzero elements shown

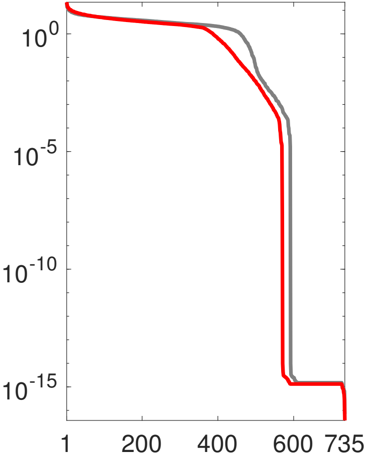

Singular values of A
(diagonal of D)

Limited data gives only part of the wavefront set

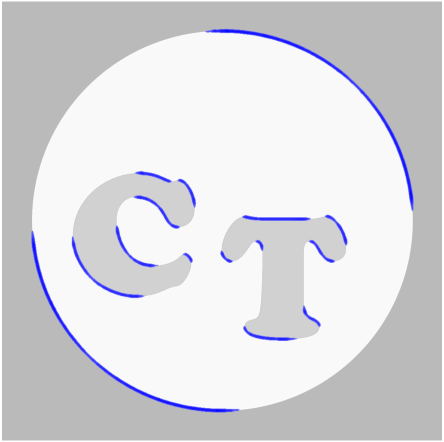

Stable part of wavefront set

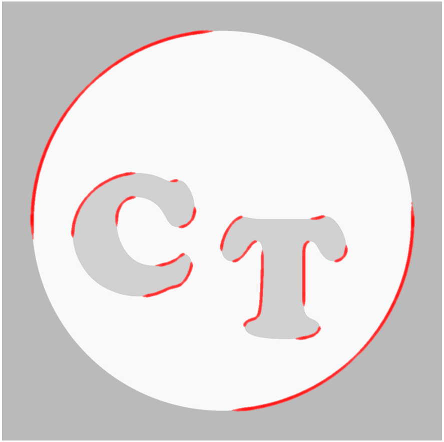

Unstable part of wavefront set

See [Greenleaf & Uhlmann 1989], [Quinto 1993], and [Frikel & Quinto 2013]

Filtered backprojection

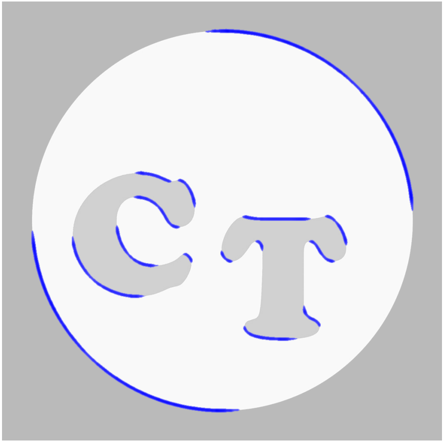

Stable part of WF set

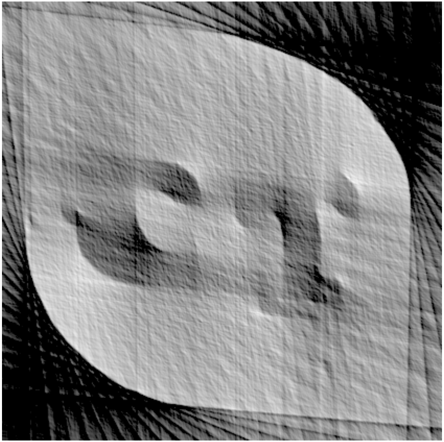

Reconstruction by FBP

Constrained total variation (TV) regularization

$$\operatorname*{arg\,min}_{f \in \mathbb{R}^n_+} \left\{ \|Af - m\|_2^2 + \alpha \|\nabla f\|_1 \right\}$$

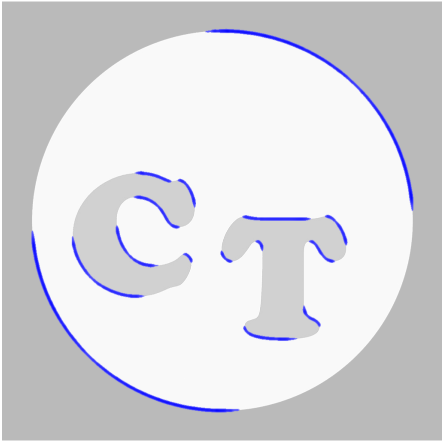

Stable part of WF set

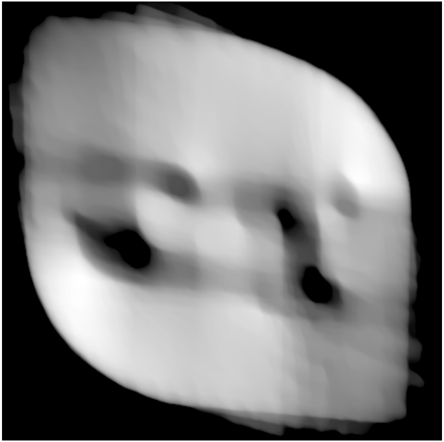

TV regularized reconstruction

Outline

The VT device was developed in 2001–2012 by

Nuutti Hyvönen
Seppo Järvenpää
Jari Kaipio
Martti Kalke
Petri Koistinen
Ville Kolehmainen
Matti Lassas
Jan Moberg
Kati Niinimäki
Juha Pirttilä
Maaria Rantala
Eero Saksman
Henri Setälä
Erkki Somersalo
Antti Vanne
Simopekka Vänskä
Richard L. Webber

Application: dental implant planning, where a missing tooth is replaced with an implant

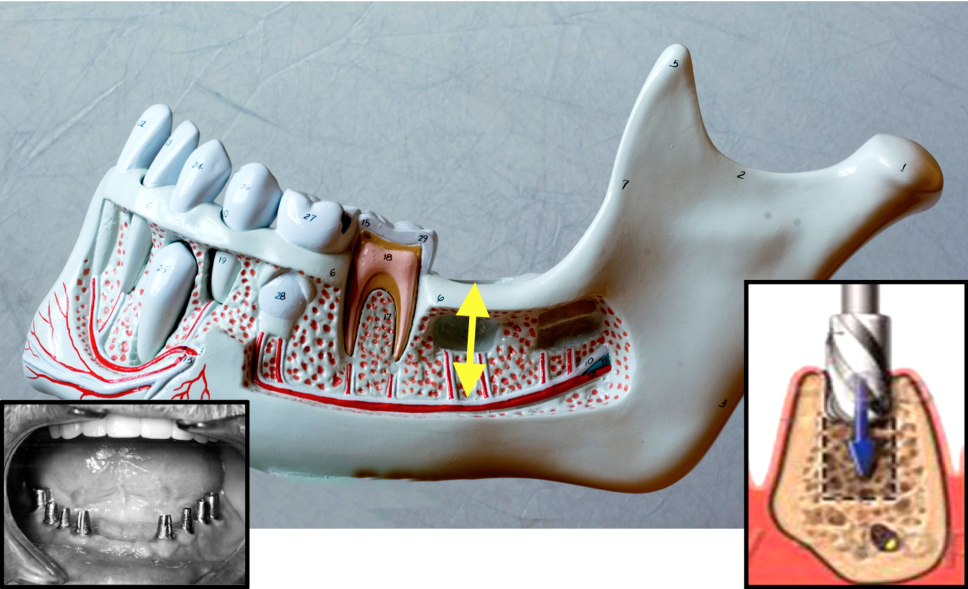

Dental X-ray imaging 100 years ago

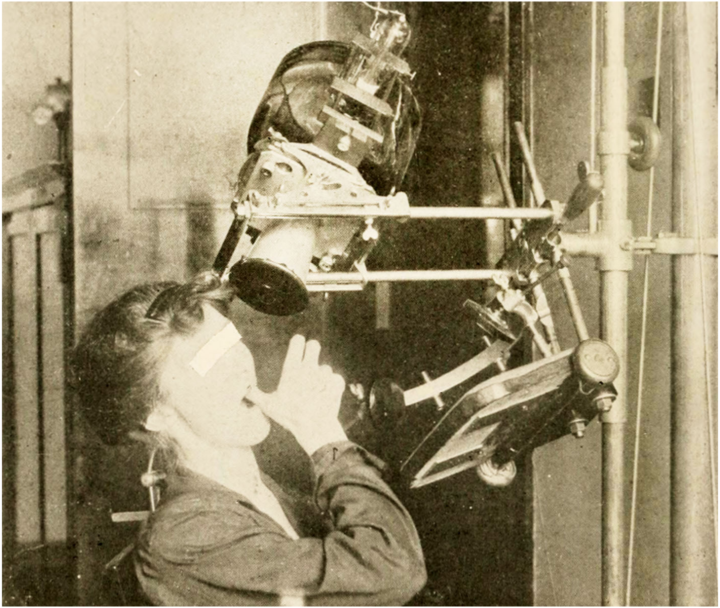

It is tedious to interpret a mosaic of overlapping intraoral X-ray images

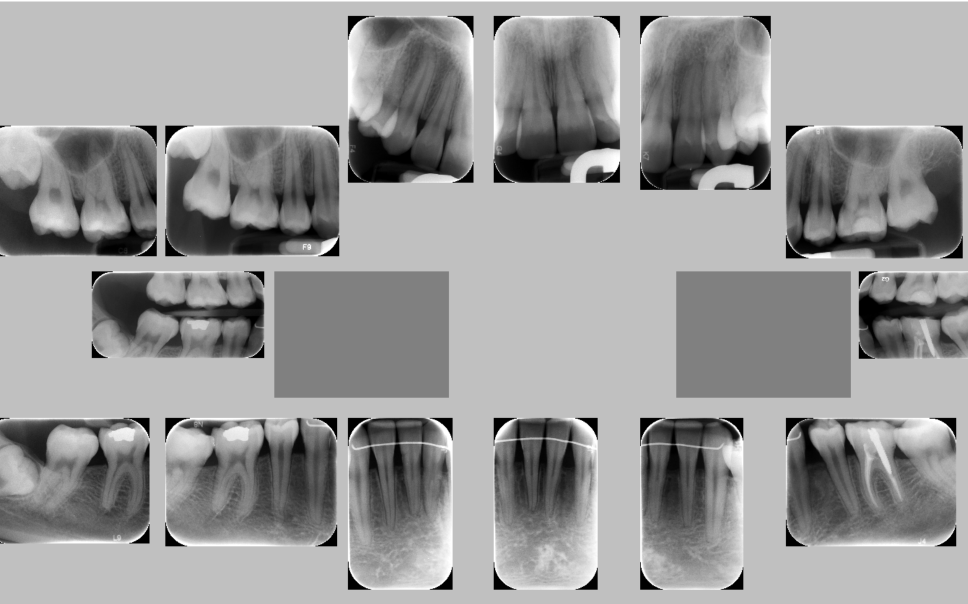

Panoramic dental imaging shows all the teeth simultaneously

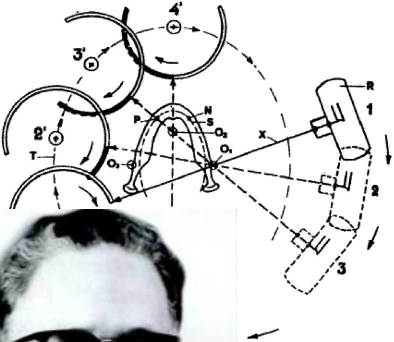

Panoramic imaging was invented by Yrjö Veli Paatero in the 1950's.

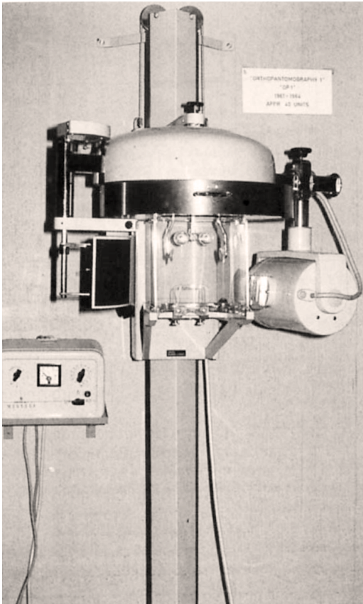

This is the classical imaging procedure of the panoramic X-ray device

https://www.youtube.com/watch?v=QFTXegPxC4U

The resulting image shows a sharp layer positioned inside the dental arc

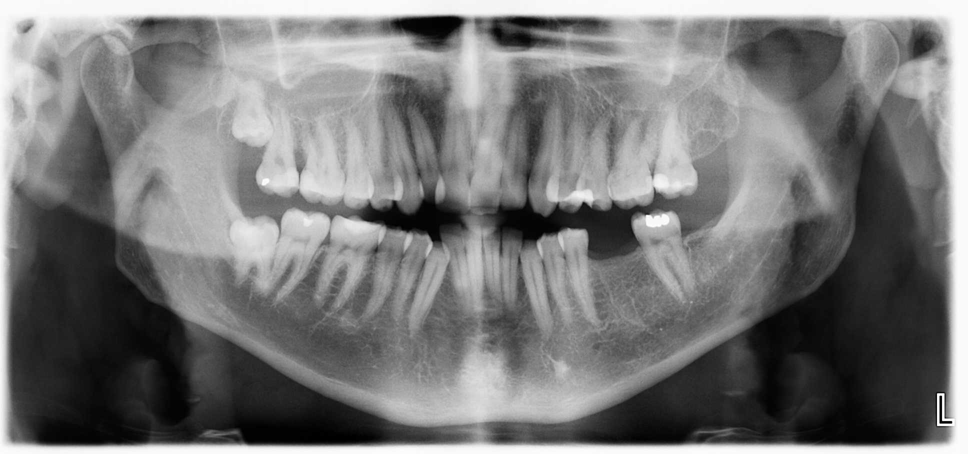

Nowadays, a digital panoramic imaging device is standard equipment at dental clinics

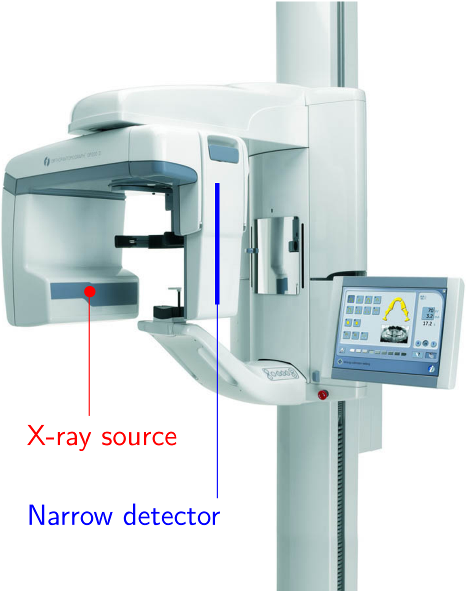

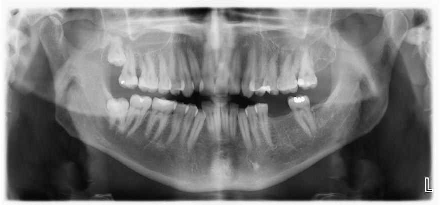

A panoramic dental image offers a general overview showing all teeth and other structures simultaneously.

Panoramic images are not suitable for dental implant planning because of unavoidable geometric distortion.

We reprogram the panoramic X-ray device so that it collects projection data by scanning

https://www.youtube.com/watch?v=motthjiP8ZQ

We reprogram the panoramic X-ray device so that it collects projection data by scanning

Number of projection images: **11**

Angle of view: **40 degrees**

Image size: **1000×1000 pixels**

The unknown vector f has **7 000 000** elements.

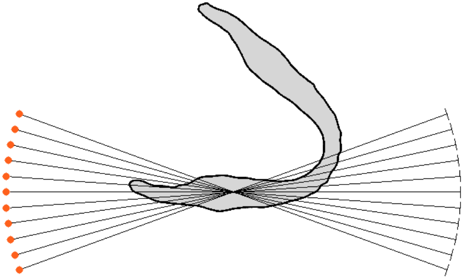

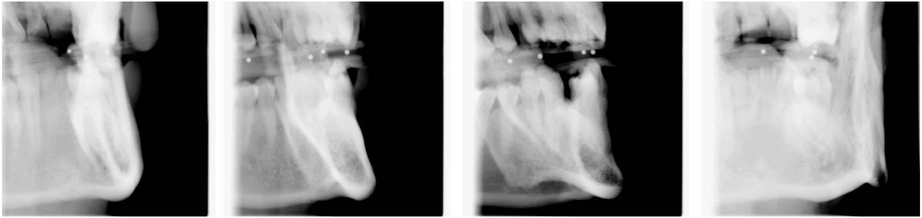

Here the CBCT reconstruction (right) gave 100 times more radiation than VT imaging (middle)

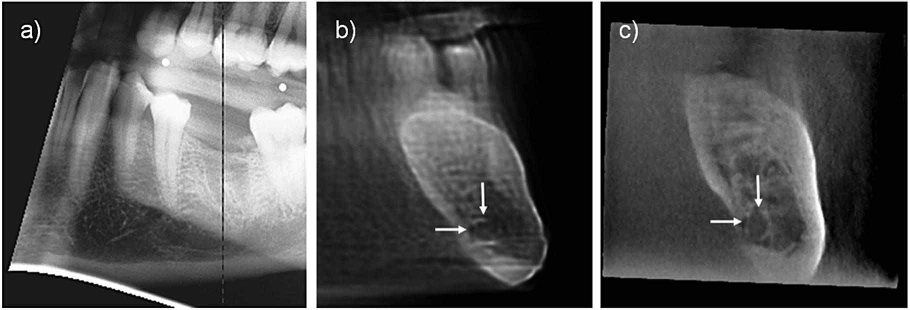

Kolehmainen, Vanne, S, Järvenpää, Kaipio, Lassas & Kalke **2006**

Kolehmainen, Lassas & S **2008**

Cederlund, Kalke & Welander **2009**

Hyvönen, Kalke, Lassas, Setälä & S **2010**

U.S. patent 7269241, thousands of VT units in use

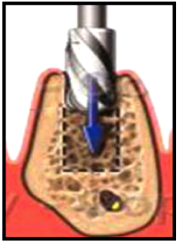

Finnish Inverse Problems Society offers open X-ray tomographic datasets

fips Finnish Inverse Problems Society

See the website https://www.fips.fi/dataset.php

The ASTRA toolbox contains important algorithms

See the website http://www.astra-toolbox.com/

[W. van Aarle, W. J. Palenstijn, J. Cant, E. Janssens, F. Bleichrodt, A. Dabravolski, J. De Beenhouwer, K. J. Batenburg, and J. Sijbers 2016]

[W. van Aarle, W. J. Palenstijn, J. De Beenhouwer, T. Altantzis, S. Bals, K. J. Batenburg, and J. Sijbers 2015]

Another great resource is Per Christian Hansen's 3D tomography toolbox TVreg

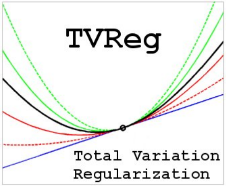

TVreg: Software for 3D Total Variation Regularization (for Matlab Version 7.5 or later), developed by Tobias Lindstrøm Jensen, Jakob Heide Jørgensen, Per Christian Hansen, and Søren Holdt Jensen.

Website: `http://www2.imm.dtu.dk/ pcha/TVReg/`

These books are recommended for learning the mathematics of practical X-ray tomography

1983 Deans: The Radon Transform and Some of Its Applications

1986 Natterer: The mathematics of computerized tomography

1988 Kak & Slaney: Principles of computerized tomographic imaging

1996 Engl, Hanke & Neubauer: Regularization of inverse problems

1998 Hansen: Rank-deficient and discrete ill-posed problems

2001 Natterer & Wübbeling: Mathematical Methods in Image Reconstruction

2008 Buzug: Computed Tomography: From Photon Statistics to Modern Cone-Beam CT

2008 Epstein: Introduction to the mathematics of medical imaging

2010 Hansen: Discrete inverse problems

2012 Mueller & S: Linear and Nonlinear Inverse Problems with Practical Applications

2014 Kuchment: The Radon Transform and Medical Imaging

Thank you for your attention!